

Characterization and evolution of tropospheric plumes from Lascar and Villarrica volcanoes, Chile

T. A. Mather,¹ V. I. Tsanev,² D. M. Pyle,¹ A. J. S. McGonigle,² C. Oppenheimer,² and A. G. Allen³

Received 20 April 2004; revised 22 July 2004; accepted 2 August 2004; published 4 November 2004.

[1] Direct sampling (filter pack and impactor) and remote sensing (ultraviolet spectroscopy and Sun photometry) of the plumes of Lascar and Villarrica volcanoes, Chile, reveal that both are significant and sustained emitters of SO₂ (28 and 3.7 kg s⁻¹, respectively), HCl (9.6 and 1.3 kg s⁻¹, respectively), HF (4.5 and 0.3 kg s⁻¹, respectively) and near-source sulfate aerosol (0.5 and 0.1 kg s⁻¹, respectively). Aerosol plumes are characterized by particle number fluxes (0.08–4.0 μm radius) of ~10¹⁷ s⁻¹ (Lascar) and ~10¹⁶ s⁻¹ (Villarrica), the majority of which will act as cloud condensation nuclei at supersaturations >0.1%. Impactor studies suggest that the majority of these particles contain soluble SO₄²⁻. Most aerosol size distributions were bimodal with maxima at radii of 0.1–0.2 μm and 0.7–1.5 μm. The mean particle effective radius (R_{eff}) ranged from 0.1 to 1.5 μm, and particle size evolution during transport appears to be controlled by particle water uptake (Villarrica) or loss (Lascar) rather than sulfate production.

INDEX TERMS: 0305 Atmospheric Composition and Structure: Aerosols and particles (0345, 4801); 0322 Atmospheric Composition and Structure: Constituent sources and sinks; 0365 Atmospheric Composition and Structure: Troposphere—composition and chemistry; 8409 Volcanology: Atmospheric effects (0370); 8494 Volcanology: Instruments and techniques; **KEYWORDS:** volcanoes, degassing, aerosol sulphur dioxide, sulphate, Llaima

Citation: Mather, T. A., V. I. Tsanev, D. M. Pyle, A. J. S. McGonigle, C. Oppenheimer, and A. G. Allen (2004), Characterization and evolution of tropospheric plumes from Lascar and Villarrica volcanoes, Chile, *J. Geophys. Res.*, 109, D21303, doi:10.1029/2004JD004934.

1. Introduction

[2] Volcanoes are important natural sources of atmospheric gases and particles. Volcanic emissions can strongly perturb atmospheric chemistry and Earth's energy balance when released in larger eruptions but also contribute to the background time-averaged composition of the atmosphere. Volcanic sulfate aerosol emitted directly from volcanic vents [e.g., Allen *et al.*, 2002; Mather *et al.*, 2003a], or resulting from atmospheric SO₂ oxidation, plays a key role in the atmosphere's general radiative balance [Graf *et al.*, 1997], and may also cause climate perturbation when large quantities of volcanogenic SO₂ enter the stratosphere [e.g., Robock, 2000]. Due to the altitude and location of their emissions, volcanic effects on the atmosphere can be disproportionately large compared to their source strength [e.g., Chin and Jacob, 1996; Graf *et al.*, 1997; Stevenson *et al.*, 2003]. Near-source volcanic particles also contribute significantly to the cycling of many trace metals and metalloids between

the Earth's interior and the atmosphere [e.g., Mather *et al.*, 2003b].

[3] In order to understand the role of volcanic emissions in the troposphere it is necessary to characterize their composition, as well as the processes that occur during transport away from the source. Here we present a detailed study, carried out in January and February 2003, of the emissions from Lascar and Villarrica volcanoes in Chile. Both volcanoes are associated with the subduction of the Nazca plate. Emissions from both sources are at significant altitude (the crater rims of both volcanoes are at elevations >2500 m), and thus may experience extended atmospheric lifetimes. We deployed a range of ground-based direct sampling and remote sensing techniques to constrain the chemical composition and fluxes of both gaseous and particulate phases in the plumes. Parallel remote sensing measurements of SO₂ and particles at different distances from the emission source allowed us to study evolution of the plumes during transport downwind to some extent. We also assess here the consistency in results obtained by the different techniques.

1.1. Lascar Volcano

[4] Lascar (5592 m; 23.37°S, 67.73°W) is a calc-alkaline stratovolcano located in the Central Andes of northern Chile, east of the Salar de Atacama (Figure 1). Since 1984 the activity of Lascar has been characterized by cycles [Oppenheimer *et al.*, 1993; Matthews *et al.*, 1997; Wooster

¹Department of Earth Sciences, University of Cambridge, Cambridge, UK.

²Department of Geography, University of Cambridge, Cambridge, UK.

³School of Geography, Earth and Environmental Sciences, University of Birmingham, Birmingham, UK.

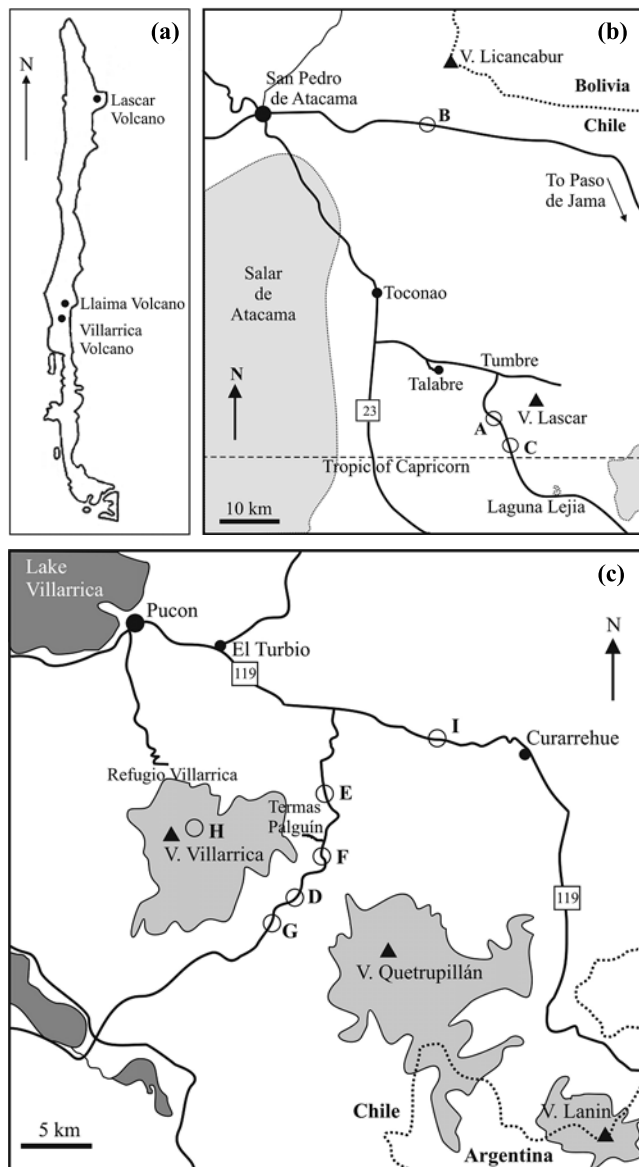


Figure 1. Maps showing the locations of Lascar, Villarrica, and Llaima volcanoes: (a) location within Chile, (b) road network surrounding Lascar Volcano (light grey areas are salt pans), and (c) road network surrounding Villarrica Volcano (dark grey areas are lakes and light grey areas are ice caps).

and Rothery, 1997; Wooster, 2001]. In each cycle a lava dome is extruded in the active crater, accompanied by vigorous high-temperature degassing through fumaroles on and around the dome, and occasional minor explosions. The dome then subsides back into the conduit, accompanied by decreasing gas output, and the cycle is completed by violent explosive activity. At the time of our field measurements, the surface of the collapsed dome at the base of Lascar's active crater was covered with blocky debris and the system was believed to be at or near the climax of the "dome subsidence phase" [Global Volcanism Network (GVN), 2003; E. Calder, personal communication, 2003]. Strong fumarolic activity was evident around the inner

crater rim. At least one minor explosion occurred during our sampling campaign.

1.2. Villarrica Volcano

[5] Villarrica (2847 m; 39.42°S, 71.93°W) is a stratovolcano situated in the southern Chilean Andes (Figure 1). At the time of measurement, Villarrica was degassing from an open vent (magma-filled conduit open to the atmosphere) within the active crater producing a persistent gas plume that drifted downwind from the volcano [Witter *et al.*, 2004]. Audible small explosions and the fall of ash and scoria around the crater rim suggested that the magma level was reasonably high in the conduit (perhaps of the order of tens of meters below the crater floor), although magma was not directly visible from the crater rim. This style of activity is commonly referred to as Strombolian and reflects the rupture of the surface of the top of the magma column by slugs of gas.

1.3. Llaima Volcano

[6] During our period of field measurements the neighboring Llaima Volcano (3125 m; 38.69°S, 71.73°W) was in a state of heightened activity with an episode of abnormally high heat release producing cracks in its ice cover [Global Volcanism Network (GVN), 2004; H. Moreno Roa, personal communication, 2003]. Some measurements were made here also.

2. Methods

2.1. Direct Sampling

2.1.1. Impactor

[7] Impactor measurements were made on the crater rims of Lascar and Villarrica, as well as at background sites (Table 1). A 10-stage micro-orifice uniform deposit impactor (MOUDI, MSP Corporation, Minneapolis, Minnesota, USA) was used in conjunction with a 12 V Charles Austin pump powered by portable 12 V 6.5 Ah batteries. At a flow rate of 30 L min⁻¹ the 50% efficiency cut off aerodynamic diameters (D_{50}) of particles collected by the 11 stages (including the inlet stage but not the outlet stage) of the impactor (in μm) are 18, 9.9, 6.2, 3.1, 1.8, 1.0, 0.55, 0.325, 0.175, 0.099 and 0.054, allowing collection of particles in eleven size fractions between 0.054 μm and >18 μm . In the field we could only obtain flow rates of 7.5–11.5 L min⁻¹, necessitating recalculation of the 50% cutoff diameters, using the approximation that the D_{50} values will be larger than those for 30 L min⁻¹ by the ratio of the square roots of the flow rates (i.e., $\sqrt{30/Q}$, where Q is the measured flow rate) (MSP Corporation, written communication, 2002). Teflon filter substrates were used on all stages of the impactor, except the outlet stage for which a quartz filter was used.

2.1.2. Filter Packs

[8] Filter pack samples were collected at Lascar summit on 23 January 2003 (sample duration \sim 20 min at \sim 14 L min⁻¹) and in the plume at the crater rim of Villarrica on 3 and 7 February 2003 (sample duration 30–60 min at \sim 15 L min⁻¹). These filter packs had four stages, a PTFE 1 μm pore size filter designed to collect all particles with high efficiency, followed by three stages of filters designed to collect gaseous species [Allen *et al.*, 2000]. Background measurements were also made at each location.

Table 1. Summary of Impactor Runs

Volcano	Run	Date in 2003	Position ^a	Start Time (Local)	Duration	Mean Measured Flow Rate, L min ⁻¹	Relative Humidity, %	Temperature, °C	Pressure, mbar	Comments
Lascar	1	23 January	Lascar summit (5455 m asl)	1503	1 hours 22 min	7.5	15–16	7–9	526	a little downwind from the crater edge, plume lofting a little overhead
Lascar	2	25 January	downwind just at foot of Lascar (4761 m asl)	1205	4 hours 10 min	10.5	22–27	11–20	575	plume overhead
Lascar: background	3	28 January	Talabre village (3257 m asl)	1905	4 hours 40 min	10	15–23	14–21	680	plume going east, i.e., not over the village
Villarrica	4	5 February	Villarrica summit (2854 m asl)	1257	2 hours 29 min	10.5	35–38	6–8	716	directly on crater rim, intermittent strong plume puffs
Villarrica: background	5	12 February	flank of Villarrica	1458	6 hours 14 min	11.5	65	19	936	in forest on volcano's flanks but not under the plume

^aAbbreviation asl represents meters above sea level.

[9] Chemical analysis of the samples from both the impactor, and filter packs, was carried out by ion chromatography (Dionex DX 500) upon return to the United Kingdom. The gaseous species SO₂, HCl, HF and HNO₃ were determined as SO₄²⁻, Cl⁻, F⁻ and NO₃⁻, respectively. The particle filters were analyzed for soluble SO₄²⁻, Cl⁻, F⁻, NO₃⁻, H⁺, K⁺, Na⁺, NH₄⁺, Ca²⁺ and Mg²⁺ (see *Mather et al.* [2003a] for a detailed description of methodology).

2.2. Remote Sensing

2.2.1. Ultraviolet Spectroscopy

[10] An Ocean Optics USB 2000 ultraviolet (UV) spectrometer was used to measure SO₂ column amounts. The spectrometer uses scattered solar radiation. At Lascar, Villarrica and Llaima, sulfur dioxide fluxes were determined by orientating the telescope of the UV spectrometer to point vertically out of a car window and using the local road networks (Figure 1) to traverse under the plume. Plume column cross sections were combined with plume speed estimates (determined by visually tracking plume puffs) to calculate fluxes. A full description of the theory and practical application of this methodology can be found elsewhere [e.g., *McGonigle et al.*, 2002, 2003].

2.2.2. Sun Photometry

[11] Sun photometers have been previously deployed in volcanological contexts to observe stratospheric aerosols from the 1982 eruption of El Chichón [*Asano et al.*, 1985] and the 1991 eruption of Pinatubo [*Asano et al.*, 1993; *Tomasi et al.*, 1997] and tropospheric aerosol from the sustained degassing of Mount Etna [*Watson and Oppenheimer*, 2000, 2001] and Kilauea [*Porter et al.*, 2002]. In this study, a hand-held Microtops II Sun photometer [*Morys et al.*, 2001] was used, which measured direct solar radiance in four channels with peak wavelengths of 440, 675, 870 and 1020 nm. Data are automatically recorded and handled by a built-in microprocessor which calculates the total optical thickness, $\tau(\lambda)$, the solar zenith angle, Z , and the air mass factor m . The channels' peak wavelength precision is ± 1.5 nm, the full width at half maximum is 10 nm, and the field of view is 2.5° (<http://www.solar.com/mtops.htm>). Measured wavelengths coincide with those recommended for retrieving information about atmospheric aerosols by the World Meteorological Organization [*Fröhlich*, 1977]. It should be noted that because the UV spectrometer measured the diffuse, zenith sky radiation, its line of sight always differed, at least slightly, from that of Sun photometer.

2.2.2.1. Theory

[12] At 440, 675, 870 and 1020 nm wavelengths, the optical thickness is derived from the Beer-Bouguer-Lambert law

$$V(\lambda) = \frac{V_o(\lambda)}{D^2} \exp[-\tau(\lambda)m], \quad (1)$$

where for each wavelength, λ (measured in nm), $V(\lambda)$ is the signal (in V) measured by the Sun photometer at λ , $V_o(\lambda)$ is the extraterrestrial signal at λ (measured in V) at mean Earth-Sun distance, D is the ratio of the Earth-Sun distance (measured in astronomical units) at the time of the

measurement to the mean Earth-Sun distance, $\tau(\lambda)$ is the total optical thickness at λ and m is the air mass factor, given by the ratio of the total atmospheric thickness along the oblique trajectory of the incoming direct solar radiation to the total vertical atmospheric thickness. The parameters $V_0(\lambda)$ are present as instrumental constants in the Microtops II memory, but can be calculated using a Langley calibration approach [Shaw, 1983; Tomasi *et al.*, 1997]. The instrument used during our field campaign was calibrated by the Solar Light Company at Mauna Loa observatory, Hawaii approximately six months prior to deployment. The relative error of $V_0(\lambda)$ was approximately 0.5% for all wavelengths. Two Langley calibrations were carried out at each location in Chile but the atmospheric conditions were not ideal for confirming the internal calibrations of the Microtops II. Our estimates differed from the internal calibrations by 0.8–1.4%. According to the detailed investigation of the Microtops II calibration stability reported by Ichoku *et al.* [2002], accepting the previous calibration performed at the Mauna Loa Observatory should not introduce significant error.

[13] At a wavelength λ , the total optical thickness recorded by the Microtops can be expressed as the sum

$$\tau(\lambda) = \tau_A(\lambda) + \tau_R(\lambda), \quad (2)$$

where $\tau_A(\lambda)$ is the aerosol optical thickness and $\tau_R(\lambda)$ is the Rayleigh optical thickness (which depends on wavelength and local pressure at the measurement site).

[14] To investigate volcanic plume aerosol properties it is necessary to make measurements both of the background atmosphere (clear from volcanic emission) and where the Sun is observed through the volcanic plume. The optical thickness of the plume ($\tau_p(\lambda)$) can then be obtained by subtracting the optical thickness of the background atmosphere ($\tau_b(\lambda)$) from the total through-plume optical thickness ($\tau_{\text{tot}}(\lambda)$),

$$\tau_p(\lambda) = \tau_{\text{tot}}(\lambda) - \tau_b(\lambda). \quad (3)$$

If it is assumed that the atmosphere remains homogeneous between the background and in-plume measurements (i.e., both measurements are made in quick succession, and close by), that the optical thickness of the “clear” atmospheric layer filled by the volcanic plume is negligible compared to $\tau_b(\lambda)$, and that the Rayleigh optical thickness ($\tau_R(\lambda)$) is approximately the same for $\tau_{\text{tot}}(\lambda)$ and $\tau_b(\lambda)$, then $\tau_p(\lambda)$ is the plume aerosol optical thickness. The quantity $\tau_b(\lambda)$ was determined from the weighted mean of near-simultaneous out of plume measurements taken during each measurement session. The accuracy of Sun photometers has been studied previously by many authors [e.g., Shaw, 1983; Schmid *et al.*, 1997; Miller *et al.*, 2001; Porter *et al.*, 2001; Ichoku *et al.*, 2002]. Following the analysis of Miller *et al.* [2001] (available at http://simbios.gsfc.nasa.gov/ye_reports.html) and taking Sun pointing errors of 0.3–0.5% [Morys *et al.*, 2001; E. M. Rollin, personal communication, 2002] we estimate the maximum standard deviation for our measured $\tau(\lambda)$ values to be 0.005 (the majority of our measurements were performed at solar zenith angles of 60°–75°), which should be multiplied by

2 to get the standard deviation of $\tau_p(\lambda)$, since this is determined by the subtraction of two measured values.

2.2.2.2. Ångström Coefficients

[15] For most atmospheric aerosols the spectral dependence of the measured aerosol optical thicknesses can be approximated as a function of two terms α and β via the empirical Ångström equation [Ångström, 1964]

$$\tau_p(\lambda) = \beta \lambda^{-\alpha}, \quad (4)$$

(expressed for a volcanic plume) where α is determined from the slope of a plot of $\log(\tau_p(\lambda))$ against $\log(\lambda)$, and β is the best fit value of $\tau_p(\lambda)$ at $\lambda = 1 \mu\text{m}$. This empirical expression can be obtained from Mie theory assuming spherical particles with constant index of refraction with particle size distribution described by an empirical power law equation with exponent $(-\nu - 1)$, where ν is the Junge parameter which depends on the aerosol type [van de Hulst, 1957]. The turbidity parameter α is equal to $\nu - 2$, and depends on the shape of the particle size distribution of aerosol particles, decreasing as particles grow. Typical values for α are 4 for molecular (Rayleigh) scattering, ~ 0 for coarse aerosol, ~ 2 for urban aerosol and $\sim 1-2$ for rural haze [Baltensperger *et al.*, 2003]. The parameter β depends on the total number of aerosol particles, the particle size distribution shape parameters and the complex index of refraction of particulate matter [Tomasi *et al.*, 1997].

2.2.2.3. Size Distributions

[16] The spectral dependence of $\tau_p(\lambda)$ describes the attenuation of solar radiation by the volcanic aerosols and provides the theoretical basis for retrieving the aerosol column particle size distribution $n_c(r)$ via a Fredholm integral equation of the first kind

$$\tau_p(\lambda) = \int_0^{\infty} \pi r^2 Q_{\text{EXT}}(2\pi r/\lambda, \tilde{m}) n_c(r) dr, \quad (5)$$

where Q_{EXT} is the extinction efficiency factor calculated from Mie scattering theory, r is the particle radius, \tilde{m} is the complex index of refraction and $n_c(r)$ is the column particle size distribution (the number of particles per unit area per unit radius interval in the vertical column through the plume) [Yamamoto and Tanaka, 1969]. Equation (5) only applies if the aerosol particles are spherical with a chemical composition constant over radius r . This assumption, experimental error and the fact that the infinite integration limits must be replaced by finite values r_{min} and r_{max} mean the inversion of equation (5) to give $n_c(r)$ from the spectral variation of $\tau_p(\lambda)$ is an ill-posed mathematical problem. Numerous mathematical techniques have been employed for this inversion: (1) numerical inversion algorithm application pioneered by Yamamoto and Tanaka [1969] using the linear inversion technique developed by Phillips [1962] and Twomey [1963] (a method later used by King *et al.* [1978], Nakajima *et al.* [1983], Nakajima and Tanaka [1988] and Dubovik and King [2000]); (2) iterative [Heintzerberg *et al.*, 1981] and analytical [Perelman and Shifrin, 1980] solutions; (3) empirical orthogonal functions [Ben-David *et al.*, 1988]; (4) analytic eigenfunction theory [Box *et al.*, 1992, 1996]; (5) repetitive genetic algorithm for

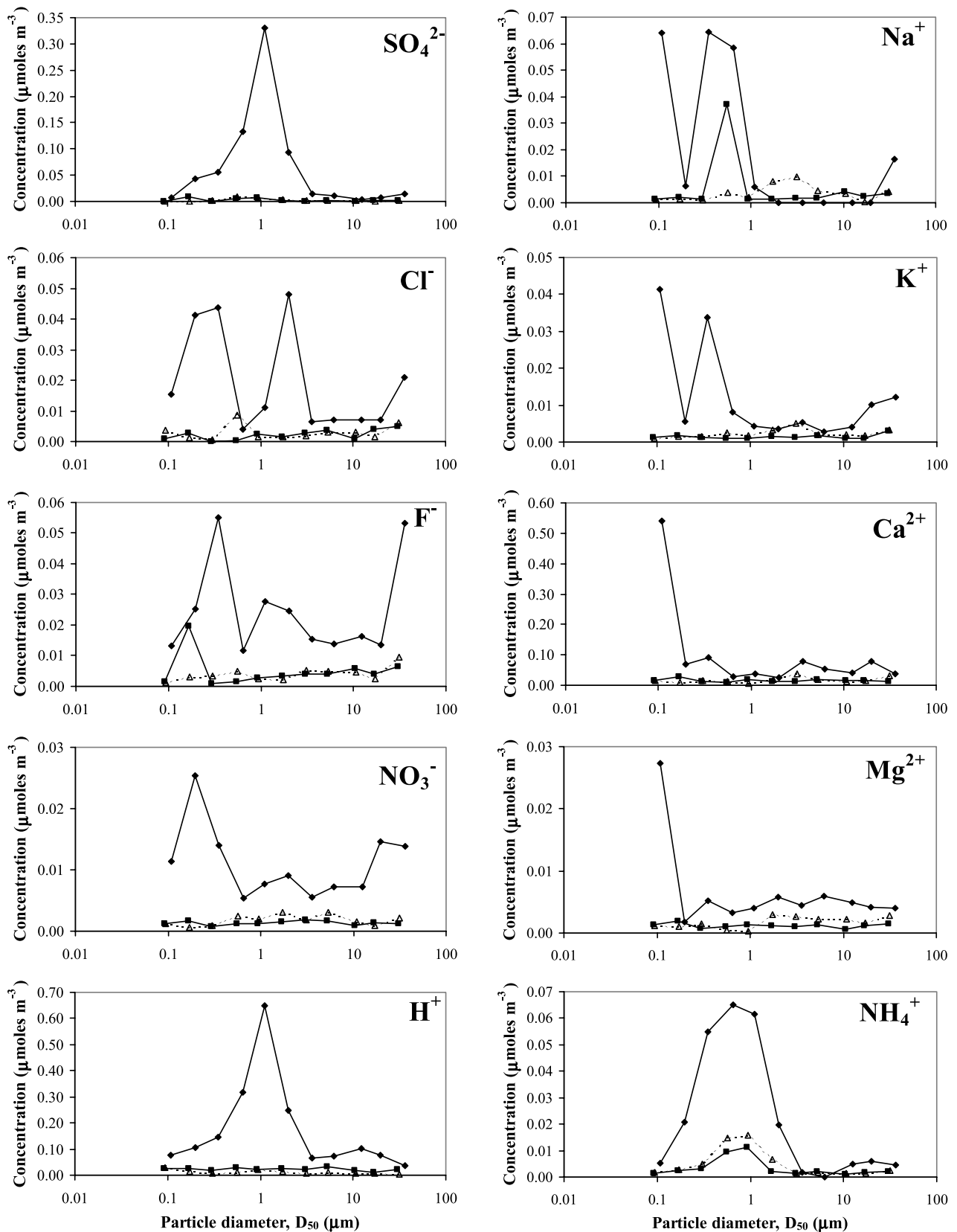


Figure 2. Variations in size-resolved speciation of the major water-soluble anions and cations in the particle phase at Lascar. Diamonds represent run 1 (summit), squares represent run 2 (in valley downwind of volcano), and triangles represent run 3 (background).

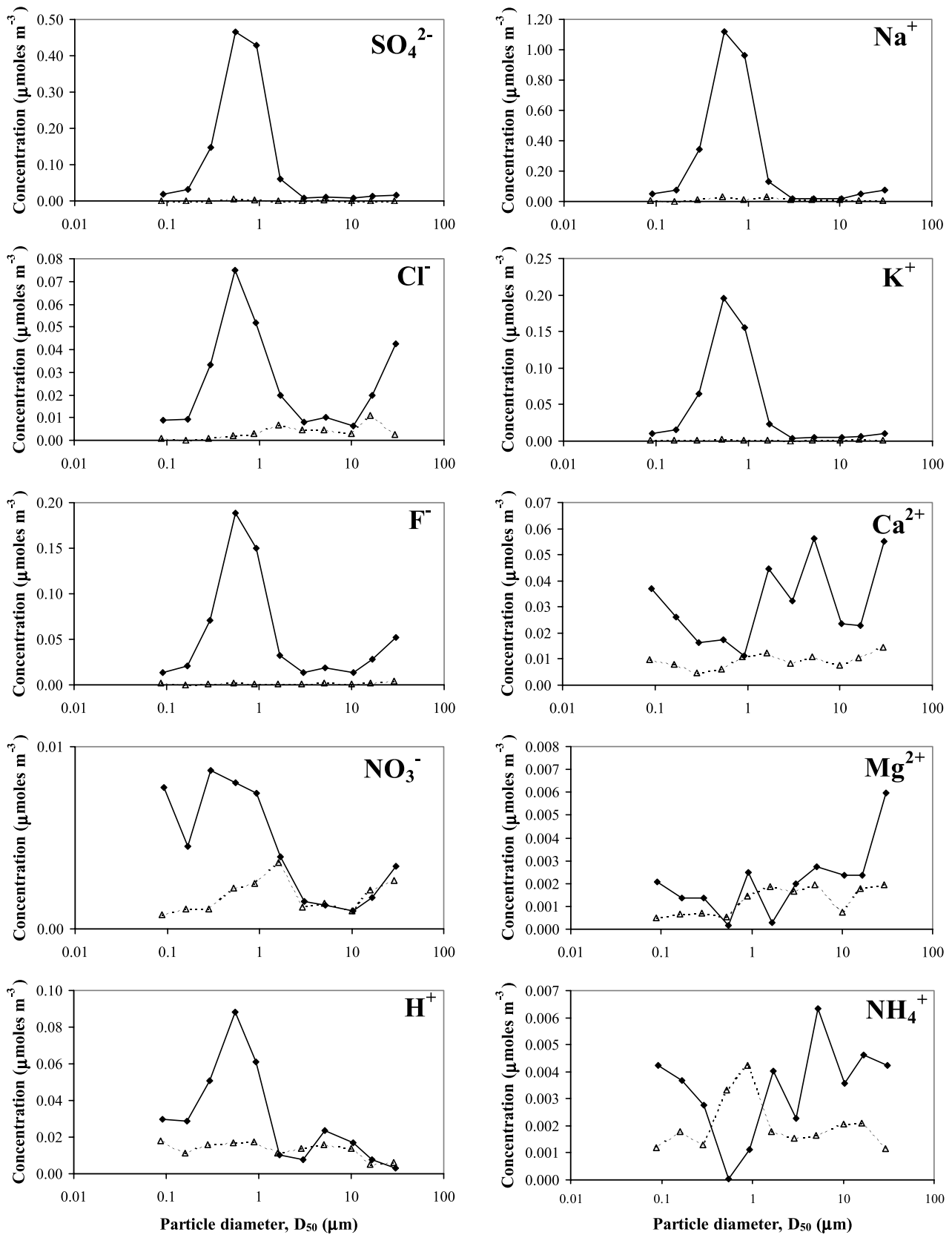


Figure 3. Variations in size-resolved speciation of the major water-soluble anions and cations in the particle phase at Villarrica. Diamonds represent run 4 (summit), and triangles represent run 5 (background).

Table 2. Summary of SO₂ Fluxes Measured by Traversing the Plume From the Main Active Crater at Each Volcano

Volcano	Date	SO ₂ Flux, kg s ⁻¹
Lascar	18 January	20.8, 27.8, 34.7, 27.8^a
Villarrica	8 February	3.2
Villarrica	12 February	6.0, 3.8, 4.2, 2.2, 2.8, 3.7^a
Llaima	6 February	6.7, 2.5
Llaima	10 February	8.1, 12.7, 6.1, 7.8, 7.3^a

^aBoldface value indicates the mean value of all the flux measurements from that volcano during the sampling campaign.

selecting the best solution [Lienert *et al.*, 2001]; and (6) selection of the best solution within a family of lognormal distributions [Porter *et al.*, 2002].

[17] Here we apply the method proposed by King *et al.* [1978], using software adapted from <http://ltpwww.gsfc.nasa.gov/crg/software.html>. This method was chosen as it has been comprehensively tested [King *et al.*, 1978; King, 1982; Jorge and Ogren, 1996; Martínez-Lozano *et al.*, 1999] and successfully used by many authors, including investigations of volcanic aerosols [e.g., Spinhirne and King, 1985; Schmid *et al.*, 1997; Tomasi *et al.*, 1997; Watson and Oppenheimer, 2000, 2001]. A modification of King *et al.*'s [1978] method [Dubovik and King, 2000] is also currently accepted within the AERONET network [Holben *et al.*, 1998]. The King *et al.* algorithm calculates the inverted column aerosol size distribution using the product of two functions: (1) the Junge distribution calculated using the estimated value of α and (2) a modification of the Junge distribution. The algorithm then employs an iterative method, combined with reevaluation of the solutions using equation (5) in order to identify the smoothest solution that coincides most closely with the measured spectral dependency of $\tau_p(\lambda)$. This process is equivalent to a constrained linear inversion with automatic selection of the Lagrange multiplier. The refractive index is one of the inputs for the King *et al.* inversion. Although this varies with aerosol composition we decided to choose one value and apply it to all retrievals as it is hard to make definite assumptions regarding aerosol composition and in order to facilitate fair comparison of other calculated aerosol properties. The value of 1.44–0.0i was chosen as that for a concentrated (>60%) sulfate and water solution [Palmer and Williams, 1975; Tang and Munkelwitz, 1994; Krotkov *et al.*, 1997]. This value was used successfully in previous studies of the near-source plume of Mount Etna [Watson and Oppenheimer, 2001] and reflects the prevalence of SO₄²⁻ in the aerosol phase (Figures 2 and 3), the concentrations implied by application of the Aerosol Inorganics Model (AIM) (see discussion in section 3.6) and the potential presence of low levels of silicate or other insoluble

species in even relatively passively emitted near-source volcanic plumes [Watson and Oppenheimer, 2001]. Examination of the Lascar and Villarrica impactor data (Figures 2 and 3) suggests, with caution, that the particles are mainly between ~0.1 and 6.0 μm in diameter, although pure water droplets will not show up in these measurements and high blank values on the final quartz filter meant that the composition of particles <0.1 μm in diameter was very difficult to assess. Generally, setting the minimum radius for the retrieval as 0.08 μm and the maximum radius as 4.0 μm (the maximum range allowed by the program) gave good coincidence between the measured and the reevaluated aerosol optical thickness (from the retrieved particle size distribution). This range was altered at some locations in order to improve agreement. The particle size distribution was retrieved in six size bins between the minimum and maximum radii. The King *et al.* method allows the number of the inverted radii to exceed the number of the measured optical thicknesses as the shape of the size distribution is partially assumed (from the Junge parameter) in the inversion [Jorge and Ogren, 1996]. As many measurements as possible were made at each location in order to allow greater confidence in the averages presented here.

3. Results and Discussion

3.1. Sulfur Dioxide Fluxes

[18] SO₂ fluxes from Lascar, Villarrica and Llaima are summarized in Table 2. At Lascar, three successful traverses were made the morning after a minor explosion (occurring ~23:00 local time). While it is possible that the flux of SO₂ from the volcano was elevated that morning, the flux estimate obtained is very similar to that measured for Lascar in 1989 by Andres *et al.* [1991] of 27 kg s⁻¹ (2300 Mg d⁻¹). There has been little change in the general activity of Lascar since this time [Matthews *et al.*, 1997; GVN, 2003]. Our results for Villarrica (mean 3.7 kg s⁻¹) are similar to previous estimates of 3.0 kg s⁻¹ (260 ± 170 t d⁻¹) and 5.4 kg s⁻¹ (460 ± 260 t d⁻¹) for 2000 and 2001 respectively [Witter *et al.*, 2004], consistent with the sustained and steady degassing of Villarrica over this period. This persistent SO₂ flux from Villarrica should be incorporated into compilations of volcanoes that persistently release SO₂ such as that of Andres and Kasgnoc [1998]. To our knowledge our measurements at Llaima represent the first SO₂ flux measurements from this volcano. Although Llaima appeared to be in an unusually high state of activity when at the time of our measurements [GVN, 2004], should such degassing prove persistent, our mean estimate of 7.3 kg s⁻¹ would place Llaima among the 15 most prolific persistent

Table 3. Concentration of Major Water-Soluble Cations and Anions in the Gas and Particle Phases of the Plumes

Volcano ^a	Mean Concentration, $\mu\text{moles m}^{-3}$													
	Gas				Particles									
	SO ₂	HCl	HF	HNO ₃	SO ₄ ²⁻	Cl ⁻	F ⁻	NO ₃ ⁻	Na ⁺	K ⁺	Mg ²⁺	Ca ²⁺	NH ₄ ⁺	H ⁺
Lascar: background	0.30	0.31	1.40	0.06	0.09	0.05	0.02	0.04	0.06	0.02	0.03	0.13	0.13	0.01
Lascar: in-plume	74.01	44.75	37.95	5.61	0.85	0.02	0.20	0.05	0.05	0.04	0.02	0.21	0.04	0.20
Villarrica: background	0.57	0.79	1.73	1.63	0.03	0.02	0.01	0.01	0.03	0.01	0.01	0.07	0.01	0.07
Villarrica: in-plume	218.86	122.11	64.26	1.84	5.04	0.03	0.46	0.06	2.77	0.71	0.06	0.20	0.01	8.49

^aNumbers of samples are as follows: Lascar background (one sample), Lascar in-plume (two samples), Villarrica background (two samples), and Villarrica in-plume (four samples). For a discussion of the HNO₃ levels at both volcanoes, see Mather *et al.* [2004].

Table 4. Mean Molar Ratios to SO₂ (X/SO_2) and Fluxes of Major Cations and Anions in Gas and Particle Phases of the Plumes

	Gas					Particles ^a					
	HCl	HF	HNO ₃	SO ₄ ²⁻	Cl ⁻	F ⁻	NO ₃ ⁻	Na ⁺	K ⁺	Mg ²⁺	Ca ²⁺
Molar ratio (X/SO_2)	0.61 ± 0.08	0.52 ± 0.2	0.074 ± 0.40	0.01 ± 0.005	0.0003 ± 0.0003	0.003 ± 0.001	0.001 ± 0.0003	0.001 ± 0.0007	0.0005 ± 0.0004	0.0002 ± 0.0001	0.003 ± 0.002
Flux, ^b kg s ⁻¹	9.61	4.51	2.04	0.48	0.0044	0.022					
Molar ratio (X/SO_2)	0.59 ± 0.14	0.23 ± 0.12	0.012 ± 0.007	0.02 ± 0.01	0.0002 ± 0.0001	0.002 ± 0.001	0.001 ± 0.0006	0.009 ± 0.005	0.0023 ± 0.001	0.0003 ± 0.0001	0.002 ± 0.001
Flux, ^b kg s ⁻¹	1.25	0.26	0.04	0.11	0.0004	0.002		0.013	0.0053		0.004

^aNH₄⁺ is not included as it is probably not of volcanic origin.

^bFluxes are calculated by converting the molar ratios to mass ratios and multiplying by the SO₂ fluxes measured from the two volcanoes (Table 2). Fluxes are quoted only for species that are conclusively above background in Table 3.

emitters of volcanic SO₂ globally according to the compilation of *Andres and Kasgnoc* [1998].

3.2. Fluxes of Other Chemical Components

[19] Tables 3 and 4 summarize the filter pack results obtained at each volcano. Table 4 summarizes the molar ratios of plume species to SO₂ and uses the measured SO₂ fluxes (plus mass ratios calculated from the molar ratios) to calculate fluxes for other gas and particle constituents of Lascar and Villarrica's plumes. These first measurements from Lascar show that it is a significant source of HCl, HF and particulate SO₄²⁻. Other soluble species were below detection limits. Villarrica is also a significant source of HCl, HF and particulate SO₄²⁻. For Villarrica, the X/SO_2 ratios for HCl and HF are marginally higher than those measured in 2001 by *Witter et al.* [2004] of 0.39 and 0.09 (molar ratios), respectively. However, their flux estimates (HCl: 1.18 kg s⁻¹ and HF: 0.15 kg s⁻¹) are similar. Villarrica is also a significant source of particulate SO₄²⁻, Na⁺ and K⁺. This is similar to open-vent degassing at Masaya Volcano, Nicaragua, where SO₄²⁻, Na⁺ and K⁺ (as well as H⁺) were the most prevalent soluble species measured in the plume particles [*Mather et al.*, 2003a]. Near-source sulfate is emitted from both Lascar and Villarrica in particles of a similar size (0.5–1 μm diameter) and with a similar SO₄²⁻/SO₂ molar ratio (0.01 and 0.02, respectively) to those from Masaya Volcano, Nicaragua (molar ratio 0.01 [*Mather et al.*, 2003a]).

[20] Global fluxes of volcanic species other than SO₂ are usually made by assuming a typical ratio for the species to SO₂ and then scaling up using global SO₂ flux estimates (extrapolated from available measurements). Thus HCl and HF source strengths have been previously estimated at 0.4–11 × 10¹² and 0.06–6 × 10¹² g yr⁻¹, respectively, by *Symonds et al.* [1988], or 1.2–170 × 10¹² and 0.7–8.6 × 10¹² g yr⁻¹, respectively, by *Halmer et al.* [2002]. From our measurements, the sustained emissions of HCl and HF from Lascar and Villarrica alone amount to 0.34 × 10¹² and 0.15 × 10¹² g yr⁻¹, respectively. This suggests that the *Halmer et al.* [2002] lower limits are more realistic than those of *Symonds et al.* [1988] and also highlights the need for further measurements in order to constrain more accurately the global volcanic emission rates of HCl and HF.

3.3. Ångström Coefficients

[21] The Ångström coefficients α and β are well recognized as useful quantities for rapid and approximate identification of aerosols [e.g., *Schmid et al.*, 1997; *Tomasi et al.*, 1997; *Watson and Oppenheimer*, 2000, 2001]. Previous studies of the Ångström coefficients of tropospheric volcanic plumes at Mount Etna have been carried out during two separate campaigns [*Watson and Oppenheimer*, 2000, 2001]. Here α ranged from -0.30 to 0.30, and β ranged from ~0.15 to 0.65 in ash-bearing plumes and α ranged from ~0.75 to 2.50, and β from ~0.00 to 0.15 in ash-free plumes. Decreasing α normally corresponded to increasing β [*Watson and Oppenheimer*, 2000]. Below we compare the Ångström coefficients from Lascar and Villarrica with those previously calculated for Etna, discuss something of the properties of Ångström coefficients, compare them with results from retrievals of aerosol size distributions and

Table 5. Summary of Lascar Sun Photometer Measurements of Ångström Coefficients

Date in January 2003	Time, UT	Position ^a	Distance to Crater, km	Approximate Plume Age, min	In-Plume Weighted Mean		Regression β Versus α^b	Correlation Coefficient
					α	β		
15	~1040 ^c	Talabre	~20	2	1.48	0.04	not significant	
15	~1220	Tumbre	~10	30 ^d	0.77	0.02	$-0.009\alpha + 0.025$	-0.76
16	~1040 ^c	Talabre	~20	2	0.19	0.10	$0.163\alpha + 0.110^e$	+0.48
16	~1040 ^c	Talabre	~20	2	0.19	0.10	$-0.151\alpha + 0.172$	-0.74
18	~1040 ^c	road to Laguna Lejia	~10	2	1.39	0.03	$-0.026\alpha + 0.065$	-0.59
18	~1300 ^f	road to Laguna Lejia (A)	~10	12	0.51	0.23	$-0.601\alpha + 0.541$	-0.91
19	~1430 ^f	Jama Road (B)	~45	150 ^d	2.37	0.01	$-0.006\alpha + 0.024$	-0.96
28	~1040 ^c	Talabre	~20	2	0.30	0.04	$0.165\alpha + 0.049^e$	+0.73
28	~1040 ^c	Talabre	~20	2	0.30	0.04	$-0.037\alpha + 0.066$	-0.63
28	~1300 ^f	road to Laguna Lejia (C)	~10	30	1.83	0.01	$-0.007\alpha + 0.023$	-0.85
28	~1300 ^f	road to Laguna Lejia (C)	~10	30	1.62	0.05	$-0.104\alpha + 0.217$	-0.54
28	~1300 ^f	road to Laguna Lejia (C)	~10	30	1.91	0.03	$-0.032\alpha + 0.088$	-0.97
29	~1455 ^f	road to east of Tumbre	~5	15 ^d	1.64	0.01	$-0.005\alpha + 0.019$	-0.88
29	~1545 ^f	Tumbre	~10	30 ^d	1.59	0.02	$-0.014\alpha + 0.040$	-0.95
29	~1915 ^f	route 23 (south of Toconao)	~30	100 ^d	1.50	0.01	$-0.003\alpha + 0.011$	-0.86

^aLetters A–C refer to sites in Figure 1.

^bFor all quoted regressions at Lascar, there was correlation using the *t* test at significance level 1%.

^cSunrise through the plume is indicated.

^dAge is hard to determine accurately as wind speed was very low.

^eValues of α become negative.

^fThese measurements were in conjunction with SO₂ measurements.

discuss their usefulness in terms of gaining first-order information about the properties of a volcanic aerosol.

3.3.1. Lascar

[22] The mean α values obtained for Lascar's plume range from 0.19 to 2.37, and mean β values range from 0.01 to 0.23 (Table 5). All except two of our α values were greater than 0.30 and all our β values except one were less than 0.15, consistent with visual observations that the plume was free of ash and larger particles. The largest α value corresponds to the most distal plume measurements (made on the Jama Road, marked B in Figure 1b) suggesting a decrease in particle size with plume age. The smallest α values are from two of the sets of sunrise data (location indicated as Talabre in Table 5). The most likely explanation is that the particles are larger in the nocturnal plume (because of decreased temperature and increased relative humidity) as observed by Mather *et al.* [2003a] in the plume of Masaya Volcano, Nicaragua. We generally observed a negative correlation between α and β (Table 5), although with large variations in the slope of the linear regression α against β . Where $\alpha < 0$, the correlation between α and β becomes positive. Particles scatter light most efficiently if $2\pi r$ is of a similar magnitude to the wavelength of the light, λ . When $\alpha > 0$, the dependence of τ on λ is dominated by the smaller particles (i.e., $\lambda < 1 \mu\text{m}$) as α increases; hence β generally decreases. Conversely when $\alpha < 0$, the dependence of τ on λ is dominated by the larger particles, so as α becomes more negative, particles $> 1 \mu\text{m}$ become increasingly dominant, which also tends to decrease β . This is illustrated by the sunrise measurements through the plume on 16 January (Figure 4a–4c), where we observed two different aerosol regimes as the Sun rose. The Sun first rose through a region where α and β are negatively correlated suggesting that small particles dominate (comparison with other plume measurements and visual observations suggest that this is the volcanic plume). Then it passed through an aerosol where $\alpha < 0$ and α and β are positively correlated

suggesting that coarser ($> 1 \mu\text{m}$) particles dominate. Visual observations at the time suggest that the second aerosol was cirrus cloud. Cirrus may contain ice crystals with radii $> 10 \mu\text{m}$ which may deviate significantly from spherical shape [e.g., Kärcher, 2003; Yang *et al.*, 2003]. The weighted means of all data with $\alpha > 0$ for sunrise on 16 and 28 January are 0.35 and 0.38 respectively. Here the Ångström coefficients identify different types of aerosol.

[23] The different slopes of the linear regressions (Table 5) reflect the variable homogeneity of the plume during each set of measurements. If the plume is inhomogeneous (e.g., puffing) then while the particle size distribution of the aerosol, and hence α , remains fairly constant, the values of τ at each wavelength may vary considerably. Since β is the best fit value for $\tau(\lambda = 1 \mu\text{m})$, β may vary greatly compared to α . This effect is particularly clear in the results from site 2 of the plume transect (Figure 5a) made on 28 January (Figure 5b) where there was a large synchronous variation of the total optical thickness at each wavelength (Figure 5a), as the plume swung overhead (clear from SO₂ levels in Figure 5c). Hence β varies greatly and almost independently of α . As can be seen from Figures 5d and 5e large variations in α are associated with thin plume, while in the dense plume (i.e., at higher SO₂ concentrations) α only varies slightly while β follows SO₂ concentrations closely.

3.3.2. Villarrica

[24] Mean α for Villarrica's plume ranges from 0.39 to 2.76, while mean β ranges from 0.00 to 0.24 (Table 6), consistent with our visual observations that the plume was generally ash-free. Trends in α and β with distance are hard to discern. Downwind measurements showed the same negative correlation between α and β as at Lascar. Summit measurements show considerable scatter in plots of α against β (e.g., Figure 6). This was again due to the high level of plume puffiness at the summit. During plume puffs, β can vary greatly while α (related to the particle size

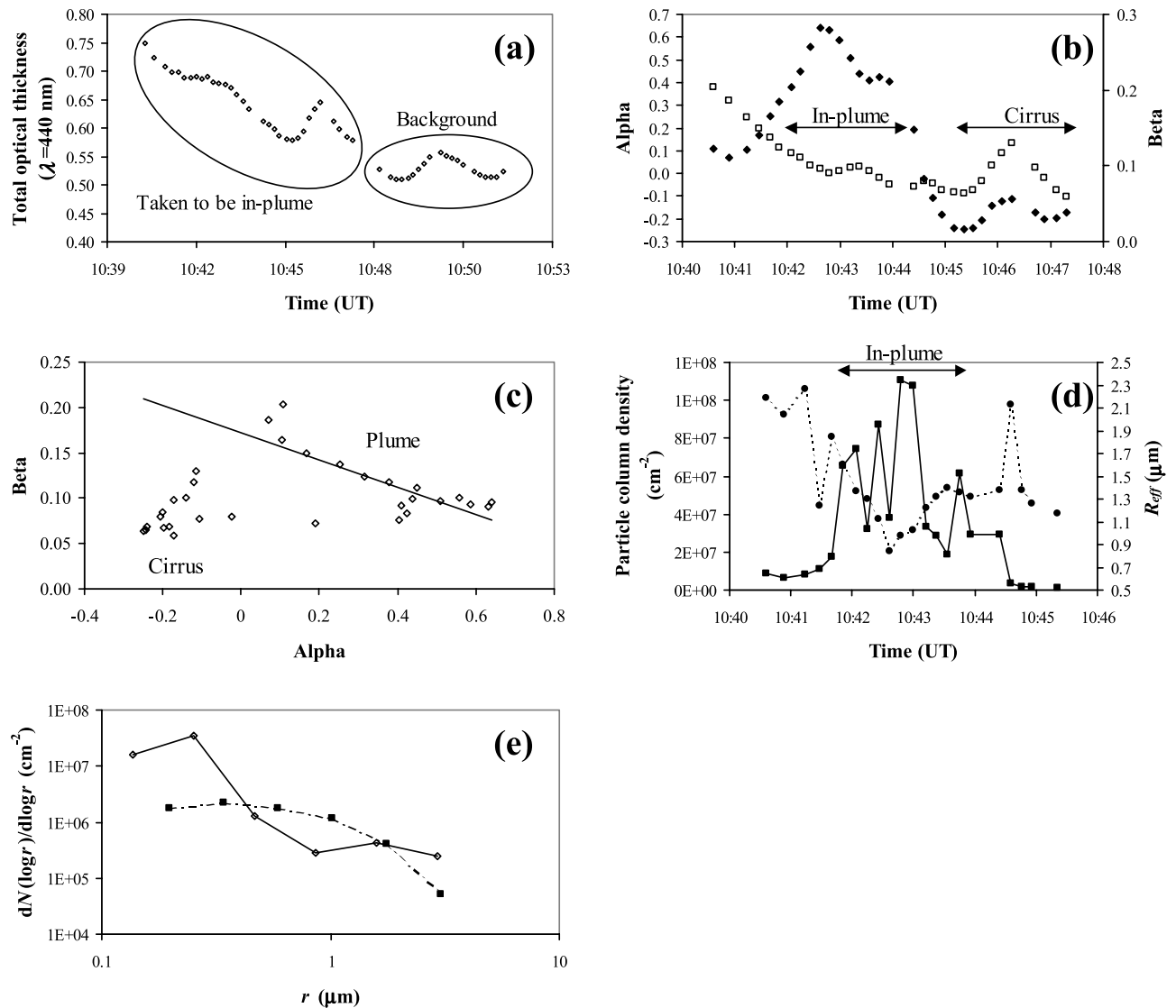


Figure 4. Results from sunrise through Lascar's plume 16 January 2003. (a) Variation of total optical thickness at wavelength 440 nm with time. (b) Variation of α and β with time for the "taken to be in plume" section. Diamonds represent α ; squares represent β . (c) A plot of α versus β . (d) Variation of particle column density and effective radius with time. Solid line represents particle numbers; dashed line represents R_{eff} . (e) Example particle number distributions. Diamonds represent inside volcanic plume ($\alpha = 0.41$); squares represent outside plume, believed to be through cirrus cloud ($\alpha = -0.11$; r_{min} had to be increased to $0.15 \mu\text{m}$ to get the retrieval to work). All times are quoted as universal time (UT).

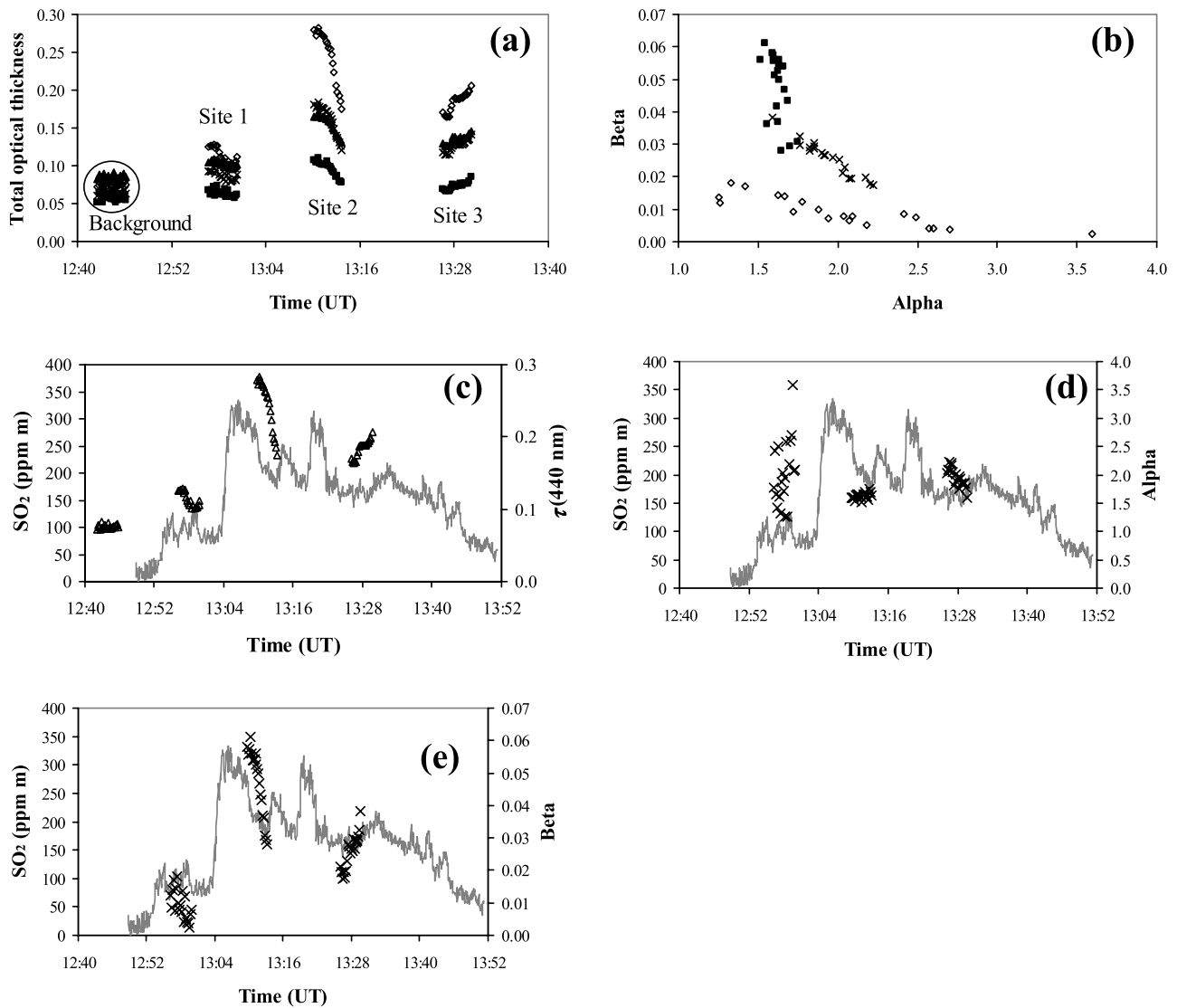


Figure 5. The results of a transect across Lascar's plume on 28 January (around position C in Figure 1b). (a) Variation of total optical thickness with time at the background site and the three different positions under the plume. Diamonds represent $\tau(440 \text{ nm})$, crosses represent $\tau(675 \text{ nm})$, triangles represent $\tau(870 \text{ nm})$, and squares represent $\tau(1020 \text{ nm})$. (b) A plot of α versus β . Diamonds represent site 1, squares represent site 2, and crosses represent site 3. (c) Variation of SO₂ column and total optical thickness at 440 nm with time. Line represents SO₂; triangles represent $\tau(440 \text{ nm})$. Times of $\tau(440 \text{ nm})$ values are adjusted by 30 s to account for a noted discrepancy between the clocks for the two sets of measurements and some time lag due to the geometries of measurement. (d) Variation of α and SO₂ with time. Line represents SO₂; crosses represent α . (e) Variation of β and SO₂ with time. Line represents SO₂; crosses represent β .

Table 6. Summary of Villarrica Sun Photometer Measurements of Ångström Coefficients

Date in February 2003	Time, UT	Position ^a	Distance to Crater, km	Approximate Plume Age, min	Weighted Mean In-Plume Results ^b	
					α	β
3	~1500–1800	summit (H)	~0	~1	1.54	0.03
3	~1500–1800	summit (H)	~0	~1	1.90	0.03
3	~1500–1800	summit (H)	~0	~1	1.24	0.03
5	~1600–1900	summit (H)	~0	~1	1.62	0.01
5	~1600–1900	summit (H)	~0	~1	0.92	0.02
7	~1200–1530	ascending ice cap ~2300 m altitude	~2	~5	1.21	0.07
7	~1200–1530	ascending ice cap ~2300 m altitude	~2	~5	0.97	0.05
7	~1700–1900	summit (H)	~0	~1	1.49	0.24
7	~1700–1900	summit (H)	~0	~1	1.81	0.16
7	~1700–1900	summit (H)	~0	~1	1.82	0.13
8	~1400–1700	road past Termas Palguín ^c	~10	~15–30	0.39	0.01
8	~1400–1700	road past Termas Palguín ^c	~10	~15–30	2.76	0.01
8	~1400–1700	road past Termas Palguín (D) ^c	~10	~15–30	1.13	0.04
8	~1400–1700	road past Termas Palguín (D) ^c	~10	~15–30	1.59	0.03
8	~1400–1700	road past Termas Palguín (D) ^c	~10	~15–30	1.04	0.01
8	~1400–1700	road past Termas Palguín (D) ^c	~10	~15–30	0.57	0.02
8	~1400–1700	road past Termas Palguín ^c	~10	~15–30	1.10	0.00
8	~1400–1700	road past Termas Palguín ^c	~10	~15–30	1.05	0.01
8	~1400–1700	road past Termas Palguín (E) ^c	~10	~15–30	1.51	0.02
8	~1400–1700	road past Termas Palguín (F) ^c	~10	~15–30	1.27	0.02
8	~1400–1700	road past Termas Palguín (G) ^c	~10	~15–30	1.19	0.03
8	~1400–1700	road past Termas Palguín ^c	~10	~15–30	1.70	0.01
8	~1400–1700	road past Termas Palguín ^c	~10	~15–30	0.97	0.01
9	~1620–1915	summit (H) ^c	~0	~1	1.35	0.07
9	~1620–1915	summit (H) ^c	~0	~1	2.21	0.02
9	~1620–1915	summit (H) ^c	~0	~1	1.18	0.04
9	~1620–1915	summit (H) ^c	~0	~1	1.04	0.04
12	~1550–1600	highway 119 between El Turbio and Curarrehue (I) ^c	~20	~40–70	0.95	0.01
12	~1550–1600	highway 119 between El Turbio and Curarrehue (I) ^c	~20	~40–70	0.63	0.01

^aLetters D–I refer to sites in Figure 1.

^bDifferent values are for different measurement runs below the plume. Multiple sets of measurements were taken at each site during each sampling period.

^cLocation is in conjunction with SO₂ measurements.

distribution) varies very little. At low β values (i.e., thin plume) α ceases to be representative of the plume and hence has a high degree of scatter. Figure 6 suggests that plume α on 9 February was ~2.5. Similar plots suggest α was ~1.5 on 7 February, and ~2 on 3 February, when the plume appeared more condensed. Enhanced particle growth in the plume on these 2 days could account for the lower α values.

3.4. Comparison of Ångström Coefficients and Retrieved Aerosol Characteristics

[25] Table 7 summarizes the results from successful Sun photometer retrievals (some were unsuccessful as the plume signal was too low). A measure of the size distribution characteristics is provided by the surface weighted mean or effective radius (R_{eff}), evaluated as

$$R_{\text{eff}} = \frac{\int_{r_{\text{min}}}^{r_{\text{max}}} n_c(r)r^3 dr}{\int_{r_{\text{min}}}^{r_{\text{max}}} n_c(r)r^2 dr}. \quad (6)$$

This quantity is important when determining the radiative effects of aerosols. For example, models for the stratosphere suggest that when $R_{\text{eff}} > 2 \mu\text{m}$, aerosols cause a net

“greenhouse effect,” while for $R_{\text{eff}} < 2 \mu\text{m}$ the albedo effect dominates [e.g., Lacis *et al.*, 1992]. R_{eff} is also very sensitive to changes in the size distribution. Particle column densities (particles cm^{-2}) were also calculated by integrating $dN(r)/dr$ over the six different size bins for which $dN(r)/dr$ was retrieved. The particle column density and the R_{eff} variation with time as the Sun rose through Lascar’s plume on 16 January are plotted in Figure 4d. The R_{eff} follows a pattern consistent with that shown by the parameter α (Figure 4b), with maximum α coinciding with minimum R_{eff} and α decreasing, while R_{eff} increases,

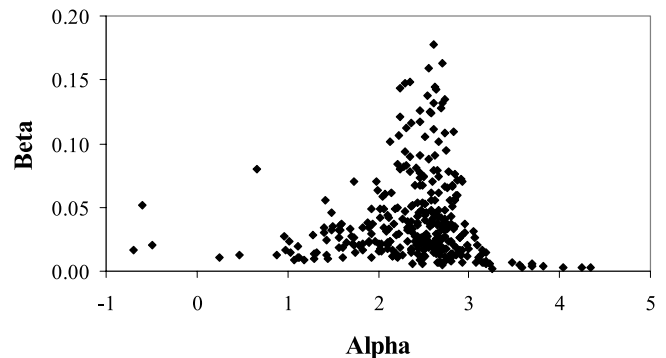


Figure 6. A plot of the Ångström coefficients from data taken at Villarrica’s summit on 9 February 2002.

Table 7. Summary of Successful Sun Photometer Retrieval Sites and Where Applicable Parallel SO₂ Measurements

Date in 2003	Description ^a	Approximate Plume Age, min	Mean R_{eff} , ^b μm	Mean Particle Column Density, ^c cm^{-2}	Mean Particle/Mass of SO ₂ Ratio		Flux	
					By Particle Mass ^d	By Particle Number, ^e kg^{-1}	Kilograms per Second	Particles per Second ^c
<i>Lascar</i>								
15 January	sunrise	2	0.53 ± 0.10 (11)	2.7×10^7				
16 January ^f	sunrise	2	1.44 ± 0.40 (22)	3.5×10^7				
18 January ^g	Laguna Lejia Road (A)	12	1.47 ± 0.35 (12)	4.1×10^7	2.79 ± 1.00 (6)	$(3.0 \pm 0.4) \times 10^{15}$	77.4	8.2×10^{16}
19 January	Jama Road (B)	150 ^h	0.18 ± 0.03 (13)	6.8×10^7	0.12 ± 0.03 (12)	$(4.2 \pm 3.1) \times 10^{15}$	3.4	1.2×10^{17}
28 January ⁱ	Laguna Lejia Road (C)	30	0.09 ± 0.01 (17)	2.2×10^8	0.11 ± 0.01 (2)	$(2.5 \pm 2.2) \times 10^{15}$	3.0	7.0×10^{16}
<i>Villarrica</i>								
8 February	Palguin Road (D)	~15–30	0.28 ± 0.04 (15)	2.3×10^8	0.19 ± 0.04 (10)	$(7.9 \pm 3.1) \times 10^{15}$	0.7	2.9×10^{16}
8 February	Palguin Road (E)	~15–30	0.28 ± 0.10 (20)	1.1×10^8	0.18 ± 0.09 (5)	$(1.3 \pm 0.7) \times 10^{16}$	0.7	4.6×10^{16}
8 February	Palguin Road (F)	~15–30	0.28 ± 0.13 (11)	1.4×10^8	0.16 ± 0.07 (5)	$(1.2 \pm 0.1) \times 10^{16}$	0.6	4.2×10^{16}
8 February	Palguin Road (G)	~15–30	0.32 ± 0.15 (10)	2.1×10^8	0.53 ± 0.34 (8)	$(2.6 \pm 1.0) \times 10^{16}$	2.0	9.6×10^{16}
9 February	summit (H)	~1	0.13 ± 0.01 (193)	2.1×10^9	0.03 ± 0.02 (76)	$(4.6 \pm 3.0) \times 10^{15}$	0.1	1.7×10^{16}
12 February	Curarrehue Road (I)	~40–70	0.47 ± 0.33 (7)	1.5×10^7	0.09 ± 0.10 (2)	$(8.3 \pm 7.2) \times 10^{14}$	0.3	3.1×10^{15}
12 February	Curarrehue Road (I)	~40–70	0.51 ± 0.48 (15)	2.9×10^7	0.09 ± 0.10 (2)	$(8.3 \pm 7.2) \times 10^{14}$	0.3	3.1×10^{15}

^aLetters A–I refer to sites in Figure 1.

^bNumbers in parentheses show number of successful retrievals that mean R_{eff} and the particle column density are based on.

^cError estimates are not included for particle column density as significant scatter is expected in these measurements due to plume puffiness, etc.

^dNumbers in parentheses show number of good measurement time overlaps that mean particle/mass SO₂ ratios are based on.

^eParticles of 0.08–4.0 μm in radius.

^fCirrus cloud in background may have influenced the R_{eff} . Figure 4 suggests that R_{eff} in-plume is $\sim 0.8 \mu\text{m}$.

^gHad to increase r_{min} to 0.15 μm to get the inversions to work.

^hHard to determine accurately as wind speed was very low.

ⁱHad to reduce r_{max} to 1.5 μm to get the inversions to work.

through the plume's dilute edges. The transition from positive to negative α results in a complete change in the particle size distribution (Figure 4e). The particle column density rises roughly until the optical path of direct sunlight intersected the center of the plume and then decreases through the diffuse plume edge. Its variation with time shows only slight correspondence with β (Figure 4b). Comparison of Tables 5 and 7 similarly shows that mean values of α and R_{eff} for the same location show good correspondence (e.g., minimum R_{eff} on the Jama Road coincides with maximum α). Beta shows less correspondence with the retrieved aerosol parameters. At Villarrica (comparison of Tables 6 and 7) the correspondence between α and R_{eff} is less apparent with little difference between the α values calculated from measurements at the summit and those made on the Palguin road (plume age ~ 30 min), although the R_{eff} values do show a significant difference. Beta values, however, appear to be generally greater at the summit than at the downwind sites, perhaps reflecting the order of magnitude decreases in particle column density between the summit and downwind.

[26] Ångström coefficients can be calculated with much greater ease and speed than performing full inversions. Our comparisons show that they are a useful first-order method (especially for larger data sets) for extracting information from measurements such as those presented here, but that they should be used with caution because of their complex relationship with aerosol characteristics.

3.5. Particle Size Distributions

[27] Apart from measurements taken on 18 January (see section 3.6), or when the Sun rose behind cirrus cloud (e.g., Figure 4e), the majority of the retrieved size distributions for both volcanic plumes were bimodal with maxima at radii

0.1–0.2 μm and 0.7–1.5 μm . Others showed more “Junge-like” distributions with particle concentrations simply decreasing with increasing radius (Figure 7). Volcanic aerosol size distributions are typically multimodal, even in the absence of a larger ash fraction [e.g., *Watson and Oppenheimer*, 2001]. Previously, volcanic aerosol plumes have been observed to be trimodal [*Hobbs et al.*, 1982, 1991; *Watson and Oppenheimer*, 2000, 2001]. Since we only measured four wavelengths to input into the retrieval, we only felt justified to retrieve $dN(\log r)/d\log r$ values for six radii; therefore it may be that our size distributions show insufficient detail for three modes to be identified. Impactor data suggest that the majority of SO₄²⁻ and other chemical components are carried in the larger of the two modes identified from the Sun photometer retrievals. These particles are in the accumulation mode, and can experience extended atmospheric lifetimes. The smaller particles may be related to the ultrafine mode that has been identified previously in volcanic plumes [e.g., *Ammann and Burtscher*, 1993]. These ultrafine particles are thought to be present on the nanoscale. Our retrievals only give information on particles down to $\sim 0.1 \mu\text{m}$ in radius.

[28] The Aerosol Inorganics Model is a chemical thermodynamic model of aerosols of composition H⁺-NH₄⁺-Na⁺-SO₄²⁻-NO₃⁻-Cl⁻-H₂O, enabling the distribution of water and ions to be calculated between liquid, solid and vapor phases for ambient conditions. Application of AIM III (available at <http://mae.ucdavis.edu/~wexler/aim/model3/model3a.htm>) [*Clegg et al.*, 1998] to our impactor data from Lascar's summit (using H⁺ and Na⁺ to adjust for charge balance and the measured relative humidity given in Table 1) yields the mass of liquid water expected at equilibrium in each size fraction. Figure 8 shows the qualitative particle size distribution generated for Lascar

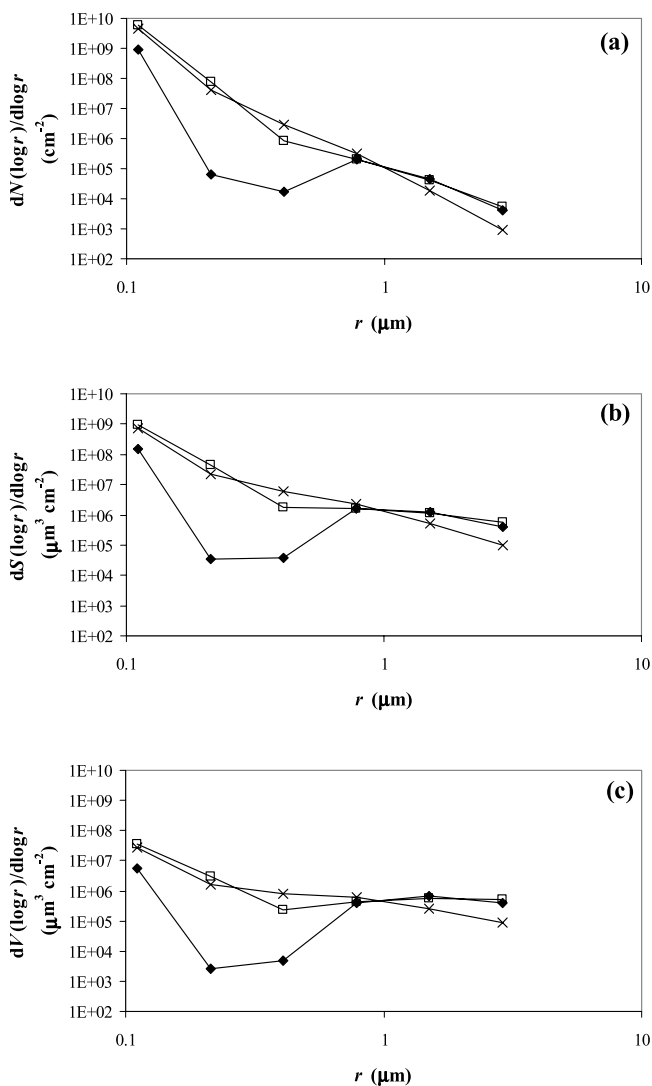


Figure 7. Example of typical (a) size, (b) surface area and (c) volume distributions for most retrieved plume measurements.

assuming that the bulk of particle volume is accounted for by the liquid H_2O and H_2SO_4 . This generates a bimodal size distribution similar to that retrieved from the Sun photometer measurements suggesting good qualitative agreement between the direct measurements and remote sensing data.

3.6. Particle Fluxes, R_{eff} , and Plume Evolution

[29] Where the particle column density appeared to correlate with the simultaneously measured SO_2 column, as in Figure 9, the particle number flux (in the range 0.08–4.0 μm radius) was calculated from the mean ratio of particle number to SO_2 mass, and multiplying by the SO_2 fluxes from Table 2. Some adjustment had to be made to account for the time discrepancy between the Sun photometer and UV measurements because of their different lines of sight. Particle mass was calculated by integrating $dV(r)/dr$ over the different size bins, taking 1.67 g cm^{-3} as the density of sulfuric acid droplets (between water at 1.0 and pure H_2SO_4 at 1.94 g cm^{-3}). This was then used to estimate a measured particle mass flux by taking a ratio with

SO_2 in a similar way as for particle number. No attempt was made to calculate the dry mass flux as this would involve assuming in-plume relative humidity and particle composition downward neither of which was measured (other than at the crater rims).

[30] At Villarrica, particle mass fluxes range from 0.10 kg s^{-1} at the crater rim to $\sim 0.65 \text{ kg s}^{-1}$ at a plume age of 15–30 min. The particle number flux (in the range 0.08–4.0 μm radius) is of the same order of magnitude at the summit and downwind, suggesting that the increase in particle mass is not due to the nucleation of new aerosol particles followed by growth or the growth of an existing nucleation mode. This is supported by the trend in R_{eff} , which shows an increase from 0.13 μm at the summit to 0.28 μm above the Palguín Road. The mass increase is therefore due either to the coagulation of volcanic particles less than 0.08 μm in radius (and hence too small for the Sun photometer to measure) with the larger aerosol during transport condensation of new sulfate (formed by the oxidation of SO_2) onto the existing aerosol during transport (see section 3.7) or due to condensation of water onto the hygroscopic sulfate aerosol.

[31] There is good agreement between the particle/ SO_2 mass ratio calculated from the remote sensing measurements (0.03 from Table 7) and the $\text{SO}_4^{2-}/\text{SO}_2$ measured using the filter packs at Villarrica's crater rim (0.03 by mass). Sulfate accounts for the majority of the mass of ions measured in the filter packs. This suggests a reasonably dry sulfate aerosol is present at the crater rim, and we again see good agreement between remote sensing and direct measurement techniques. Application of AIM [Clegg *et al.*, 1998] to the aerosol composition at the crater rim determined from the impactor (Figure 3) and simultaneously measured relative humidity (Table 1) yields a liquid water content of the aerosol of <1%. This suggests that the mass flux calculated from the measurements made at the summit ($\sim 0.1 \text{ kg s}^{-1}$) is a reasonable approximation to the dry mass flux of particles between 0.08 and 4.0 μm radius from Villarrica. This shows good consistency with a dry mass flux of 0.6 kg s^{-1} of particles from Kilauea (with simultaneous SO_2 flux of 16.8 kg s^{-1}) also calculated using Sun photometer data [Porter *et al.*, 2002].

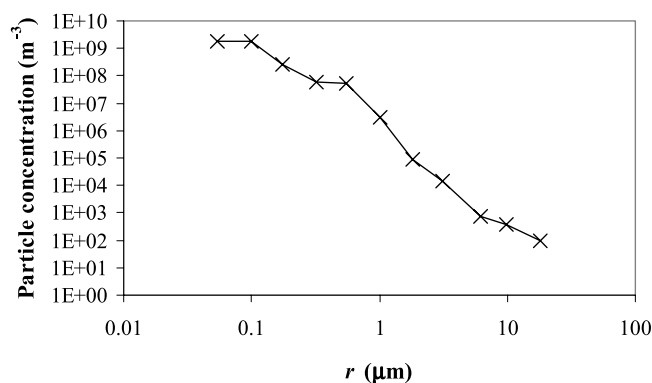


Figure 8. Particle numbers as modeled assuming water and sulphuric acid account for the majority of particle volume using the Aerosol Inorganics Model (AIM) [Clegg *et al.*, 1998].

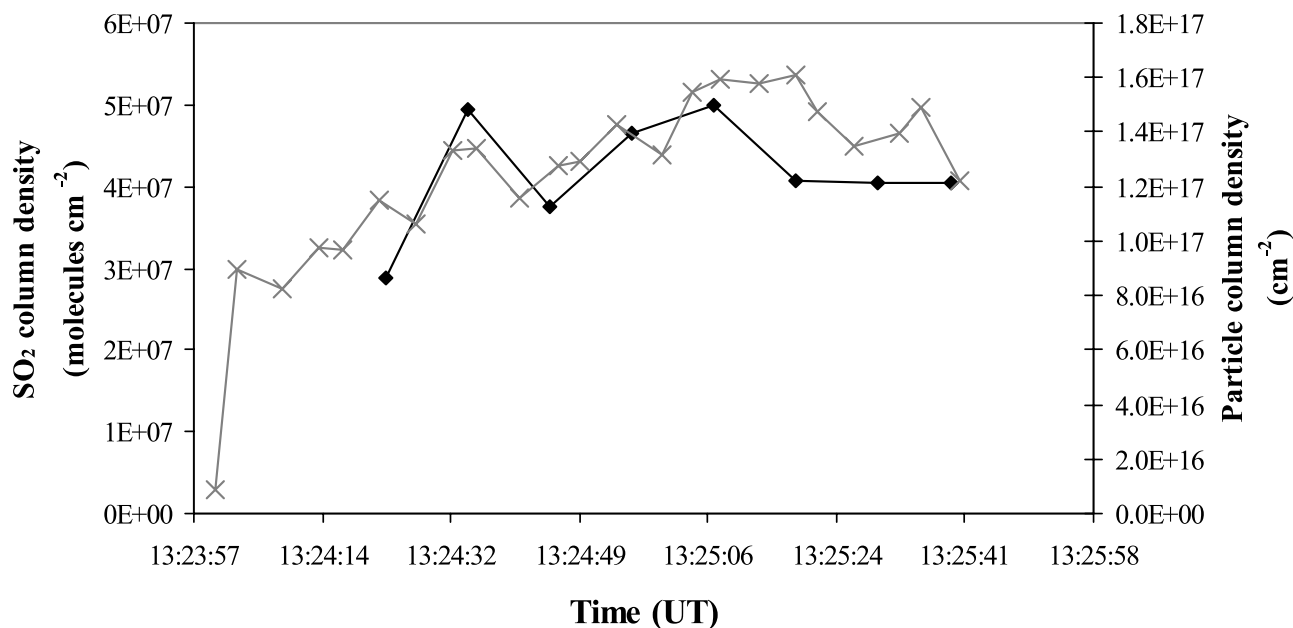


Figure 9. Example of simultaneous SO₂ and particle column measurements (taken at Lascar 18 January). Grey line represents SO₂; black line represents particles.

[32] Dilution effects are also evident as the plume travels downwind. Particle column density decreases from $\sim 10^9$ at the crater rim to $\sim 10^7$ at a plume age of 40–70 min. Assuming that the plume is ~ 10 m deep at the summit gives a summit particle concentration of $\sim 10^{12}$ particles m^{-3} , and 2×10^9 particles m^{-3} by the Curarrehue Road (assuming a plume depth of 50 m) of particles of between 0.08 and 4.0 μm in radius.

[33] Results from Lascar are more difficult to interpret. There are no clear trends in R_{eff} , particles cm^{-2} or the particle/SO₂ mass ratio with distance from the vent, although R_{eff} generally appears to decrease with plume age. This is probably due to particles condensing initially in a moist plume and then losing water (and decreasing in size) as the plume is diluted during transport in the high, dry, atmosphere of the Altiplano [Seinfeld and Pandis, 1998]. Any particle size increase due to sulfate production and condensation appears to be insignificant compared to this effect. Application of AIM [Clegg *et al.*, 1998] to the aerosol composition at the crater rim determined from the impactor (Figure 2) and simultaneously measured relative humidity (Table 1) yields a liquid water content of the aerosol of $\sim 50\%$, much higher than that calculated at Villarrica. Tracking the relative humidity and plume dilution during transport downwind would help us to understand particle evolution better. However, this would require airborne measurements, which we were unable to carry out during this campaign.

[34] Near-vent plume measurements were taken early in the day (sunrise) when temperatures were lower and more water would be condensed [see Mather *et al.*, 2003a]. There is little difference in the particle mass to SO₂ mass ratios between the results from 19 January (plume age ~ 30 min) and 28 January (plume age ~ 150 min); whereas on 18 January (plume age ~ 12 min) the particle mass to SO₂ mass ratios is an order of magnitude greater.

We suggest that meteorological conditions and not plume age controls the mass of aqueous particles present in the plume. The night before 18 January, a small explosion occurred at ~ 2300 local time producing a small ash cloud. No ash was visible in the plume the following morning, but the plume appeared more condensed. In order to successfully invert the data from that morning, r_{min} had to be increased from 0.08 μm to 0.15 μm . Resulting size distributions were strongly bimodal with one mode $< 0.2 \mu m$ in radius and one $> 3.0 \mu m$ in radius (e.g., Figure 10), with the larger size fraction probably accounted for by larger water droplets. While the mass flux is very much greater on this morning than for the other two estimates of particle mass flux, the particle number flux is reasonably similar for all three estimates. This suggests that the increased mass flux on 18 January is due to the increased condensation of water into plume particles and not due to additional ash particles.

[35] At Lascar no parallel particle and SO₂ measurements were made at the crater rim. The large discrepancy between the downwind particle to SO₂ mass ratio calculated from the

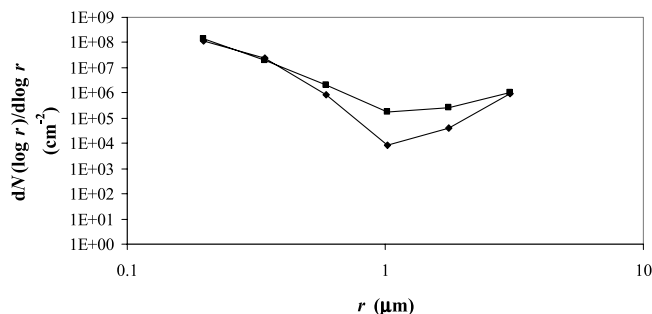


Figure 10. Particle size distributions from 18 January, the morning after a minor explosion. Diamonds represent 1324:45 UT; squares represent 1324:56 UT.

remote sensing measurements (minimum ~ 0.1) and the $\text{SO}_4^{2-}/\text{SO}_2$ mass ratio at the crater rim (0.02 from Table 4) can be accounted for by the water content of the particles.

[36] Particle number fluxes from Lascar and Villarrica are comparable to those (2×10^{15} – $4 \times 10^{18} \text{ s}^{-1}$) observed at other volcanoes during nonexplosive volcanic activity [e.g., *Stith et al.*, 1978; *Hobbs et al.*, 1982; *Radke*, 1982], although some discrepancy is to be expected because of the different size ranges measured (our particle fluxes are minimum estimates as we only measured particles of 0.08– $4.0 \mu\text{m}$ radius and did not account for the nucleation mode). Our observations suggest that the water content of a plume's aerosol phase can vary significantly during transport. Therefore for meaningful total particle mass fluxes to be quoted from volcanoes care should be taken to ensure that dry mass fluxes are measured or estimated. Much less variation was observed in our calculated particle number fluxes during plume evolution suggesting that particle number loss by sedimentation and coagulation were insignificant on these timescales. It is useful to know the size range of the particles that it was possible to measure when particle number fluxes are quoted from volcanoes.

3.7. Sulfur Dioxide Depletion

[37] Sulfur dioxide may be oxidized to sulfuric acid by a number of gas-phase, aqueous-phase or surface mechanisms, with reaction rates increasing with temperature, humidity, insolation and aerosol density [e.g., *Eatough et al.*, 1994]. Sulfur dioxide may also be lost from volcanic plumes by wet and dry deposition. Loss rates have been modeled, assuming first-order kinetics, with first-order rate constant k_1 [Möller, 1980]. Values of k_1 in tropospheric volcanic plumes have been measured as between 1.9×10^{-7} and $5.4 \times 10^{-3} \text{ s}^{-1}$ [Oppenheimer *et al.*, 1998], although the higher values may reflect SO_2 source variations, or measurement artifacts [McGonigle *et al.*, 2004]. Condensation of sulfate that is formed as SO_2 is oxidized will cause an increase in aerosol mass.

[38] At Villarrica, our remote sensing measurements suggest a particle mass increase downwind. If the aerosol mass flux increase of ~ 0.2 – 0.6 kg s^{-1} over ~ 15 – 70 min (Table 7) is due solely to SO_2 oxidation, this would require an SO_2 first-order rate loss coefficient of between 1.7×10^{-4} and $1.3 \times 10^{-5} \text{ s}^{-1}$. This is higher than most of the k_1 values summarized by Oppenheimer *et al.* [1998], but could be explained by heterogeneous oxidation either on particle surfaces or in aqueous droplets [Möller, 1980]. However, this should be treated as a maximum value for the apparent SO_2 depletion rate. As highlighted above, our observations of particle size reduction with increasing plume age at Lascar suggest that particle mass flux changes are sensitive to changes in particle water content, as well as to new sulfate production. Remote sensing alone is not a promising methodology for estimating anything more precise than maximum SO_2 depletion rates. We suggest that a better methodology would be to determine both crater rim and downwind $\text{SO}_4^{2-}/\text{SO}_2$ ratios by direct sampling methods [e.g., *Martin et al.*, 1986] and considering other loss routes such as deposition of gas and aerosol species [e.g., *Delmelle et al.*, 2001].

[39] Near-source SO_4^{2-} aerosol is present at both volcanoes, as has been observed at Masaya, Nicaragua [Allen *et*

al., 2002; *Mather et al.*, 2003a]. If the observed near-source plume sulfate results only from SO_2 oxidation, this would require apparent first-order rate coefficients (k_1) for sulfate production of $3.8 \times 10^{-5} \text{ s}^{-1}$ (at Lascar, assuming a plume age of $\sim 300 \text{ s}$), or $2.5 \times 10^{-4} \text{ s}^{-1}$ (at Villarrica, assuming a plume age of $\sim 90 \text{ s}$). The k_1 value for Lascar implies that by a plume age of $\sim 150 \text{ min}$ (e.g., at the Jama Road, B in Figure 1) the measured SO_2 flux should have dropped by $\sim 30\%$ to $\sim 20.3 \text{ kg s}^{-1}$, and the aerosol flux should have increased by $\sim 7.5 \text{ kg s}^{-1}$. Our results (particle mass flux $\sim 3 \text{ kg s}^{-1}$ measured at Jama Road) do not support this rate of particle mass gain. Results from both Lascar and Villarrica instead suggest either that the near-source sulfate production process is faster than that which prevails during longer-range transport, or that there is primary emission of sulfate from the magma. In both cases, we can consider that this near-source sulfate is present by the time that plume exits the crater. Our observations suggest that it may not be appropriate to calculate atmospheric lifetimes for SO_2 solely by measuring SO_4^{2-} particle mass fluxes downwind [e.g., *Porter et al.*, 2002]. If, as here, significant SO_4^{2-} is present in the near-source emissions, which has been directly emitted or produced by a faster SO_2 oxidation route than that which operates during transport downwind, then the presence of these SO_4^{2-} particles (of near-source origin) in the downwind measurements will lead to unrealistically high estimates of the first-order loss rate coefficients, k_1 .

3.8. Particle Composition and Cloud Condensation Nuclei (CCN) Formation

[40] The dominant chemical species in the particles of Lascar's plume are H^+ and SO_4^{2-} (Figure 2) concentrated at $\sim 1.1 \mu\text{m}$ in diameter, suggesting the presence of sulfuric acid droplets. Levels of all the other plume constituents are an order of magnitude lower (other than $\sim 0.1 \mu\text{m}$ diameter Ca^{2+}). At Villarrica, F^- , Na^+ and K^+ are present in significant concentrations in addition to H^+ and SO_4^{2-} , mainly in the ~ 0.6 and $\sim 0.9 \mu\text{m}$ diameter size fractions.

[41] In particle-free air, supersaturations of several hundred percent are necessary for the formation of water droplets. The presence of suitable particles greatly reduces the supersaturation needed. Hence particles play an important role in cloud formation. The ability of a particle to act as a nucleus for water droplet formation will depend on its size, chemical composition and the local supersaturation. Atmospheric supersaturations are typically achieved through the ascent of air parcels. Table 8 calculates the (dry) activation diameters for particles with compositions suggested by the impactor data in Figures 2 and 3. The smallest bin that we used for our aerosol size distribution retrievals from the Sun photometer had a mean radius of $\sim 0.11 \mu\text{m}$ (diameter $\sim 0.22 \mu\text{m}$). Assuming that all the aerosol from Lascar is composed of sulfuric acid, even the smallest particles retrieved from our Sun photometer measurements are larger than the critical activation diameter for 0.1% supersaturation typical of fog, unless water comprises $>80\%$ of the particle volume. Application of the AIM model [Clegg *et al.*, 1998] suggests that water makes up $\sim 60\%$ of the volume of the smaller particles, implying that all of the aerosol particle number flux that we have measured from Lascar will be activated as CCN at 0.1% supersaturation. The same is true for Villarrica, with the

Table 8. Critical Diameter for Different Solutes at Different Supersaturations Above Which Particles Are Activated as Cloud Condensation Nuclei^a

Supersaturation, ^b %	Critical Diameter, μm				
	H ₂ SO ₄	Na ₂ SO ₄	K ₂ SO ₄	NaF	KF
0.1 ^c	0.12	0.12	0.13	0.09	0.10
0.25 ^d	0.06	0.06	0.07	0.05	0.06
0.3 ^e	0.06	0.06	0.06	0.04	0.05

^aValues are calculated using equation 15.34 of *Seinfeld and Pandis* [1998, p. 789].

^bSupersaturation is the partial pressure of water vapor compared to the saturation vapor pressure of water vapor expressed as a percent. It is usually caused by the ascent of air parcels in the atmosphere.

^cMedian cloud value and typical value for fog that is quoted by *Seinfeld and Pandis* [1998, pp. 808–809].

^dLowest of the range that is quoted for continental cumulus by *Seinfeld and Pandis* [1998, p. 809].

^eLowest of the range that is quoted for maritime cumulus by *Seinfeld and Pandis* [1998, p. 809].

potential presence of NaF and KF in the particles further lowering the critical diameter. This may explain why particle growth is observed for Villarrica during transport downwind but not at Lascar. AIM predicts very little water

in the aerosol at the crater rim at Villarrica. Our impactor studies have only measured major water-soluble anions and cations; any insoluble material in aqueous particles would increase the solute effect and increase the critical diameter for CCN formation.

3.9. Sulfur Dioxide and Particle Coupling in Strombolian Pulsed Behavior at Villarrica's Summit

[42] Simultaneous SO₂ and Sun photometer measurements at the summit (Figure 11) reveal a clear pulsing pattern in the plume, similar to that described by *Witter and Calder* [2004], with “puffs” of SO₂ every ~ 2 –5 min. These pulses may relate to the ascent of large gas slugs in the conduit and the bursting of bubbles at the magma surface, but visual observations suggest that they may also relate to plume gas and aerosol accumulating in the crater before overflowing the rim. Figure 11a shows the retrieved SO₂ and particle column abundances obtained from side-by-side measurements at Villarrica's summit. While there is generally good correlation between the two sets of measurements, SO₂ levels tend to be sustained at a higher level with some troughs, while the particle numbers are generally elevated in association with elevated SO₂ levels but show

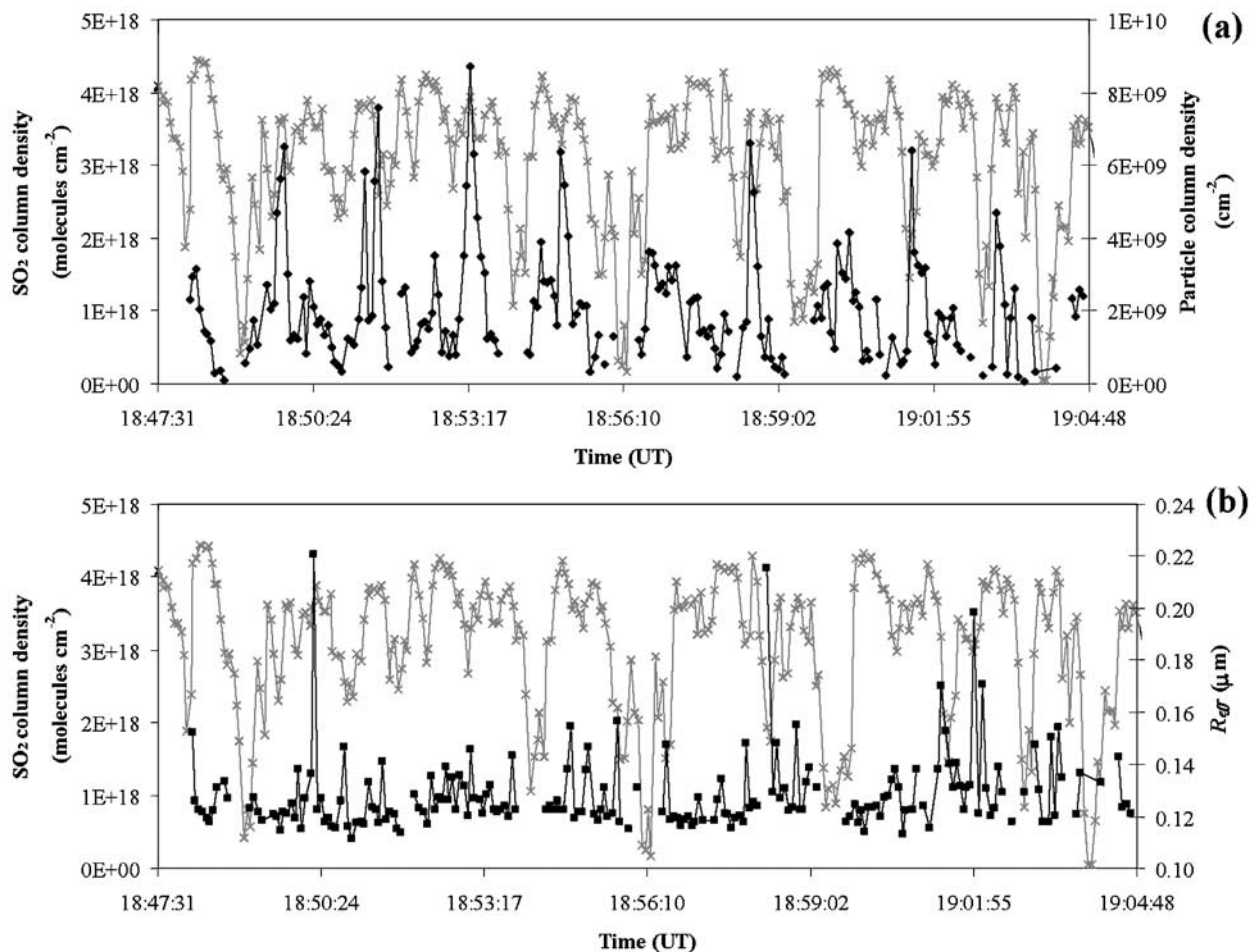


Figure 11. Variation of SO₂ as well as (a) particle column density and (b) R_{eff} , during pulsed Strombolian behavior at the summit of Villarrica. Crosses represent SO₂, diamonds represent particles, and squares represent R_{eff} .

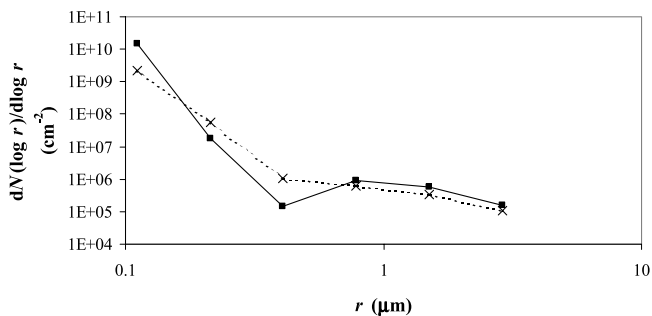


Figure 12. A comparison of the size distributions for maximum R_{eff} (dashed line and crosses) and maximum particle column density (solid line and squares) during pulsed Strombolian behavior at the summit of Villarrica.

a greater degree of spikiness. Peaks in particle number often coincide with the beginning of gas pulses (e.g., the peak at 1855:00 UT). This minor decoupling may result from slugs of gas creating particles as they break the surface of the magma pond (fine ash $<1 \mu\text{m}$ and other particles associated with bubble bursting) or by “flushing out” condensable material that may have formed just above the magma surface or in the conduit. The particle size distributions at peak particle concentrations (Figure 12) suggest that the particle enhancement is due to increased particle numbers at radius $\sim 0.1 \mu\text{m}$. These particles contain Na^+ , H^+ and SO_4^{2-} (Figure 3), suggesting that this fine aerosol forms by rapid cooling and condensation of gaseous species followed by rapid enough growth to be large enough to be measured by the Sun photometer. It may be that, combined with “flushing out” a burst of condensable material, the faster exit velocity of gases during Strombolian bursts results in the volcanic emanations experiencing a faster cooling rate altering the balance between homogeneous (forming new particles) and heterogeneous (onto existing particles) nucleation of aerosol in the plume and resulting in the formation of more particles. Further modeling and experiments are required to elucidate the processes surrounding volcanic aerosol formation. While peaks in R_{eff} (Figure 11b) could be interpreted as being due to small ash bursts, examination of the size distributions (Figure 12) shows that increases in R_{eff} are due to a decrease in the smaller size fraction and not an increase in the numbers of particles with larger radii. Further, the small ash events that were observed to accompany some Strombolian puffs had little noticeable effect on α . It appears that our measurements have not recorded any ash emissions that left the crater, probably because the majority of the coarser ash had settled out before the plume got over our measurement site on the crater rim.

4. Conclusions

[43] We have presented results from a combined deployment of direct-sampling and remote-sensing methods to study two hitherto poorly characterized volcanic plumes. Results from the remote-sensing observations are in good agreement with those from direct sampling. We have shown that both Lascar and Villarrica are significant and sustained emitters of SO_2 (28 and 3.7 kg s^{-1} , respectively),

HCl (9.6 and 1.3 kg s^{-1} , respectively), HF (4.5 and 0.3 kg s^{-1} , respectively) and near-source sulfate aerosol (0.5 and 0.1 kg s^{-1} , respectively). These fluxes of HCl and HF represent a significant fraction of the currently accepted lower limits of the global volcanic flux estimates for these species, suggesting the need for reassessment of the global volcanic halogen source to the atmosphere. Near-source SO_4^{2-} emission rates are similar to those from other volcanoes and are shown to result from a process distinct from SO_2 oxidation and SO_4^{2-} production during plume transport downwind.

[44] We have successfully combined column measurements of SO_2 and particle number density, allowing the estimation of minimum particle (0.08 – $4.0 \mu\text{m}$ radius) number fluxes of $\sim 10^{17} \text{ s}^{-1}$ for Lascar and $\sim 10^{16} \text{ s}^{-1}$ for Villarrica. Comparison of retrieved aerosol size distributions (the majority of which were bimodal with maxima at radii 0.1 – $0.2 \mu\text{m}$ and 0.7 – $1.5 \mu\text{m}$) with size resolved chemical data suggests that the majority of these particles contain soluble SO_4^{2-} . The majority of these particles will act as CCN at typical atmospheric supersaturations. These particles are also in the “accumulation” mode and so can potentially experience extended atmospheric lifetimes. The R_{eff} values measured ranged from 0.1 to $1.5 \mu\text{m}$ with particle size evolution during transport appearing to be controlled by particle water uptake or loss rather than sulfate production. Variable water content in the particle phase lead to considerable variation in the particle mass fluxes measured, especially at Lascar, suggesting that care must be taken to measure or to calculate particle dry mass fluxes from volcanoes for meaningful values to be quoted. Our examination of the Ångström coefficients from these two volcanoes found them to be consistent with those measured in the tropospheric plume from Mount Etna, and demonstrates their utility for distinguishing different types of aerosol and plume (e.g., puffy or well mixed) and as a first-order method for studying aerosol properties. Our studies of plume puffing at the crater rim of Villarrica showed that while there was generally good correlation between particle column numbers and SO_2 , there were some pulses of enhanced fine particles corresponding to “flushing out” and rapid cooling of condensable gases from the conduit by slugs of gas escaping from the magma.

[45] **Acknowledgments.** Many thanks to B. G. Mason, J. L. Permenter and V. M. Martin from Cambridge University for their help putting the funding proposal for fieldwork together and to them as well as M. L. Rampey for assistance during the sampling campaign. The authors acknowledge the Centre of Latin American Studies, Cambridge University and NERC for financial support and G. Chong (Universidad Católica del Norte, Antofagasta), H. Moreno Roa (OVDAS, Temuco), the people of Talabre village, I. M. Watson (MTU) and L. A. Rodríguez (MTU) for logistical support during the fieldwork in Chile. E.M. Rollin and other staff at NERC EPFS, Southampton University are gratefully acknowledged for all their help and advice with regard to the Microtops II instrument. S. Boreham, C. Rolfe, J. Yin and R. Lawrence are thanked for their help during the field preparation and analytical work. TM and AM acknowledge the personal financial support of the NERC, UK. TM is further sponsored by Shell and the Aerosol Society, UK. VT is funded by the EC 5th Framework project ‘DORSIVA.’ We also thank two anonymous reviewers for their efforts on our behalf.

References

Allen, A. G., P. J. Baxter, and C. J. Ottley (2000), Gas and particle emissions from Soufrière Hills Volcano, Montserrat, West Indies: Characterization and health hazard assessment, *Bull. Volcanol.*, 62, 8–19.

- Allen, A. G., C. Oppenheimer, M. Fern, P. J. Baxter, L. A. Horrocks, B. Galle, A. J. S. McGonigle, and H. J. Duffell (2002), Primary sulphate aerosol and associated emissions from Masaya Volcano, Nicaragua, *J. Geophys. Res.*, *107*(D23), 4682, doi:10.1029/2002JD002120.
- Ammann, M., and H. Burtcher (1993), Aerosol dynamics and light-scattering properties of a volcanic plume, *J. Geophys. Res.*, *98*, 19,705–19,711.
- Andres, R. J., and A. D. Kasgnoc (1998), A time-averaged inventory of subaerial volcanic sulfur emissions, *J. Geophys. Res.*, *103*, 25,251–25,261.
- Andres, R. J., W. I. Rose, P. R. Kyle, S. de Silva, P. Francis, M. Gardeweg, and H. Moreno Roa (1991), Excessive sulfur dioxide emissions from Chilean volcanoes, *J. Volcanol. Geotherm. Res.*, *46*, 323–329.
- Ångström, A. (1964), The parameters of atmospheric turbidity, *Tellus*, *16*, 64–75.
- Asano, S., M. Sakine, M. Kobayashi, and K. Murai (1985), Atmospheric turbidity and aerosol size distribution in winter at Tsukuba: Effects of the El Chichon eruption, *J. Meteorol. Soc. Jpn.*, *63*, 453–463.
- Asano, S., A. Uchiyama, and M. Shiobara (1993), Spectral optical-thickness and size distribution of the Pinatubo volcanic aerosols as estimated by ground-based sunphotometry, *J. Meteorol. Soc. Jpn.*, *71*, 165–173.
- Baltensperger, U., S. Nyeki, and M. Kalberer (2003), Atmospheric particulate matter, in *Handbook of Atmospheric Science*, edited by C. N. Hewitt and A. Jackson, pp. 228–254, Blackwell, Malden, Mass.
- Ben-David, A., B. M. Herman, and J. A. Reagan (1988), Inverse problem and the pseudoempirical orthogonal function method of solution. 1: Theory, *Appl. Opt.*, *27*, 1235–1242.
- Box, G. P., K. M. Sealey, and M. A. Box (1992), Inversion of Mie extinction measurements using analytic eigenfunction theory, *J. Atmos. Sci.*, *49*, 2074–2081.
- Box, G. P., M. A. Box, and J. Krücker (1996), Information content and wavelength selection for multispectral radiometers, *J. Geophys. Res.*, *101*, 19,211–19,214.
- Chin, M., and D. J. Jacob (1996), Anthropogenic and natural contributions to tropospheric sulfate: A global model analysis, *J. Geophys. Res.*, *101*, 18,691–18,699.
- Clegg, S. L., P. Brimblecombe, and A. S. Wexler (1998), Thermodynamic model of the system $H^+ - NH_4^+ - Na^+ - SO_4^{2-} - NO_3^- - Cl^- - H_2O$ at 298.15 K, *J. Phys. Chem. A*, *102*, 2155–2171.
- Delmelle, P., J. Stix, C. P.-A. Bourque, P. J. Baxter, J. Garcia-Alvarez, and J. Barquero (2001), Dry deposition and heavy acid loading in the vicinity of Masaya Volcano, a major sulfur and chlorine source in Nicaragua, *Environ. Sci. Technol.*, *35*, 1289–1293.
- Dubovik, O., and M. D. King (2000), A flexible inversion algorithm for retrieval of aerosol optical properties from Sun and sky radiance measurements, *J. Geophys. Res.*, *105*, 20,673–20,696.
- Eatough, D. J., F. M. Caka, and R. J. Farber (1994), The conversion of SO_2 to sulfate in the atmosphere, *Isr. J. Chem.*, *34*, 301–314.
- Fröhlich, C. (1977), WRC/PMOD Sunphotometer: Instructions for manufacture, report, World Meteorol. Organ., Geneva.
- Global Volcanism Network (GVN) (2003), Lascar, *Bull. Global Volcanism Network*, *28*(3).
- Global Volcanism Network (GVN) (2004), Llaima, *Bull. Global Volcanism Network*, *29*(2).
- Graf, H.-F., J. Feichter, and B. Langmann (1997), Volcanic sulfur emissions: Estimates of source strength and its contribution to the global sulfate burden, *J. Geophys. Res.*, *102*, 10,727–10,738.
- Halmer, M. M., H.-U. Schmincke, and H. F. Graf (2002), The annual volcanic gas input into the atmosphere, in particular into the stratosphere: A global data set for the past 100 years, *J. Volcanol. Geotherm. Res.*, *115*, 511–528.
- Heintzberg, J., H. Müller, H. Quenzel, and E. Thomalla (1981), Information content of optical data with respect to aerosol properties: Numerical studies with a randomized minimization-search-technique inversion algorithm, *Appl. Opt.*, *20*, 1308–1315.
- Hobbs, P. V., J. P. Tuell, D. A. Hegg, L. F. Radke, and M. K. Eltgroth (1982), Particles and gases in the emissions from the 1980–1981 volcanic eruptions of Mt. St. Helens, *J. Geophys. Res.*, *87*, 11,062–11,086.
- Hobbs, P. V., L. F. Radke, J. H. Lyons, R. J. Ferek, and D. J. Coffman (1991), Airborne measurements of particles and gas emissions from the 1990 volcanic eruptions of Mount Redoubt, *J. Geophys. Res.*, *96*, 18,735–18,752.
- Holben, B. N., et al. (1998), AERONET—A federated instrument network and data archive for aerosol characterization, *Remote Sens. Environ.*, *66*, 1–16.
- Ichoku, C., et al. (2002), Analysis of the performance characteristics of the five-channel Microtops II Sun photometer for measuring aerosol optical thickness and precipitable water vapor, *J. Geophys. Res.*, *107*(D13), 4179, doi:10.1029/2001JD001302.
- Jorge, H. G., and J. A. Ogren (1996), Sensitivity of retrieved aerosol properties to assumptions in the inversion of spectral optical depths, *J. Atmos. Sci.*, *53*, 3669–3683.
- Kärcher, B. (2003), Simulating gas-aerosol-cirrus interactions: Process-oriented microphysical model and applications, *Atmos. Chem. Phys.*, *3*, 1645–1664.
- King, M. D. (1982), Sensitivity of constrained linear inversions to the selection of the Lagrange multiplier, *J. Atmos. Sci.*, *39*, 1356–1369.
- King, M. D., D. M. Byrne, B. M. Herman, and J. A. Reagan (1978), Aerosol size distributions obtained by inversion of spectral optical depth measurements, *J. Atmos. Sci.*, *35*, 2153–2167.
- Krotkov, N. A., A. J. Krueger, and P. K. Bhartia (1997), Ultraviolet optical model of volcanic clouds for remote sensing of ash and sulfur dioxide, *J. Geophys. Res.*, *102*, 21,891–21,904.
- Lacis, A., J. Hansen, and M. Sato (1992), Climate forcing by stratospheric aerosols, *Geophys. Res. Lett.*, *19*, 1607–1610.
- Lienert, B. R., J. N. Porter, and S. K. Sharma (2001), Repetitive genetic inversion of optical extinction data, *Appl. Opt.*, *40*, 3476–3482.
- Martin, D., B. Ardouin, G. Bergametti, J. Carbonelle, R. Faivre-Pierret, G. Lambert, M. F. Le Cloarec, and G. Sennequier (1986), Geochemistry of sulfur in Mount Etna plume, *J. Geophys. Res.*, *91*, 12,249–12,254.
- Martínez-Lozano, J. A., M. P. Utrillas, and F. Tena (1999), Retrieval of the aerosol size distribution from spectroradiometer measurements at a coastal site in the Mediterranean Sea, *Int. J. Remote Sens.*, *20*, 2167–2182.
- Mather, T. A., A. G. Allen, C. Oppenheimer, D. M. Pyle, and A. J. S. McGonigle (2003a), Size-resolved characterisation of soluble ions in the tropospheric plume of Masaya Volcano, Nicaragua: Origins and plume processing, *J. Atmos. Chem.*, *46*, 207–237.
- Mather, T. A., D. M. Pyle, and C. Oppenheimer (2003b), Tropospheric volcanic aerosol, in *Volcanism and the Earth's Atmosphere*, *Geophys. Monogr. Ser.*, vol. 139, edited by A. Robock and C. Oppenheimer, pp. 189–212, AGU, Washington, D. C.
- Mather, T. A., A. G. Allen, B. M. Davison, D. M. Pyle, C. Oppenheimer, and A. J. S. McGonigle (2004), Nitric acid from volcanoes, *Earth Planet. Sci. Lett.*, *218*, 17–30.
- Matthews, S. J., M. C. Gardeweg, and R. S. J. Sparks (1997), The 1984 to 1996 cyclic activity of Lascar Volcano, northern Chile: Cycles of dome growth, dome subsidence, degassing and explosive eruptions, *Bull. Volcanol.*, *59*, 72–82.
- McGonigle, A. J. S., C. Oppenheimer, B. Galle, T. A. Mather, and D. M. Pyle (2002), Walking traverse and scanning DOAS measurements of volcanic gas emission rates, *Geophys. Res. Lett.*, *29*(20), 1985, doi:10.1029/2002GL015827.
- McGonigle, A. J. S., C. Oppenheimer, A. R. Hayes, B. Galle, M. Edmonds, T. Caltabiano, G. Salerno, M. Burton, and T. A. Mather (2003), Sulphur dioxide fluxes from Mount Etna, Vulcano, and Stromboli measured with an automated scanning ultraviolet spectrometer, *J. Geophys. Res.*, *108*(B9), 2455, doi:10.1029/2002JB002261.
- McGonigle, A. J. S., P. Delmelle, C. Oppenheimer, V. I. Tsanev, T. Delfosse, G. Williams-Jones, K. Horton, and T. A. Mather (2004), SO_2 depletion in tropospheric volcanic plumes, *Geophys. Res. Lett.*, *31*, L13201, doi:10.1029/2004GL019990.
- Miller, M., M. J. Bartholomew, and R. M. Reynolds (2001), Variance equations and uncertainty analysis for the Langley technique, in *In Situ Aerosol Optical Thickness Collected by the SIMBIOS Program (1997–2000), Protocols, and Data QC and Analysis*, *SIMBIOS Technical Memoranda*, edited by G. S. Fargion, R. Barnes, and C. McClain, *NASA Tech. Memo, NASA/TM-2001-209982*, 22–25.
- Möller, D. (1980), Kinetic model of atmospheric SO_2 oxidation based on published data, *Atmos. Environ.*, *14*, 1067–1076.
- Morys, M., F. M. Mims III, S. Hagerup, S. E. Anderson, A. Baker, J. Kia, and T. Walkup (2001), Design, calibration, and performance of MICROTOPS II handheld ozone monitor and Sun photometer, *J. Geophys. Res.*, *106*, 14,573–14,582.
- Nakajima, T., and M. Tanaka (1988), Algorithms for radiative intensity calculations in moderately thick atmospheres using a truncation approximation, *J. Quant. Spectrosc. Radiat. Transfer*, *40*, 51–69.
- Nakajima, T., M. Tanaka, and T. Yamauchi (1983), Retrieval of the optical properties of aerosols from aureole and extinction data, *Appl. Opt.*, *22*, 2951–2959.
- Oppenheimer, C., P. W. Francis, D. A. Rothery, R. W. Carlton, and L. S. Glaze (1993), Infrared image analysis of volcanic thermal features: Lascar Volcano, Chile, 1984–1992, *J. Geophys. Res.*, *98*, 4269–4286.
- Oppenheimer, C., P. Francis, and J. Stix (1998), Depletion rates of sulfur dioxide in tropospheric volcanic plumes, *Geophys. Res. Lett.*, *25*, 2671–2674.
- Palmer, K. F., and D. Williams (1975), Optical constants of sulfuric acid: Application to the clouds of Venus?, *Appl. Opt.*, *14*, 208–219.

- Perelman, A. Y., and K. S. Shifrin (1980), Improvements to the spectral transparency method for determining particle size distribution, *Appl. Opt.*, *19*, 1787–1793.
- Phillips, D. L. (1962), A technique for numerical solution of certain integral equations of the first kind, *J. Assoc. Comput. Mach.*, *9*, 84–97.
- Porter, J. N., M. Miller, C. Pietras, and C. Motell (2001), Ship-based Sun photometer measurements using Microtops Sun photometers, *J. Atmos. Ocean. Technol.*, *18*, 765–774.
- Porter, J. N., K. A. Horton, P. J. Mougins-Mark, B. Lienert, S. K. Sharma, E. Lau, A. J. Sutton, T. Elias, and C. Oppenheimer (2002), Sun photometer and lidar measurements of the plume from the Hawaii Kilauea Volcano Pu'u 'O'o vent: Aerosol flux and SO₂ lifetime, *Geophys. Res. Lett.*, *29*(16), 1783, doi:10.1029/2002GL014744.
- Radke, L. F. (1982), Sulphur and sulphate from Mt Erebus, *Nature*, *299*, 710–712.
- Robock, A. (2000), Volcanic eruptions and climate, *Rev. Geophys.*, *38*, 191–219.
- Schmid, B., C. Mätzler, A. Heimo, and N. Kämpfer (1997), Retrieval of optical depth and particle size distribution of tropospheric and stratospheric aerosols by means of Sun photometry, *IEEE Trans. Geosci. Remote Sens.*, *35*, 172–183.
- Seinfeld, J. H., and S. N. Pandis (1998), *Atmospheric Chemistry and Physics*, John Wiley, Hoboken, N. J.
- Shaw, G. E. (1983), Sun photometry, *Bull. Am. Meteorol. Soc.*, *64*, 4–10.
- Spinhirne, J. D., and M. D. King (1985), Latitudinal variation of spectral optical thickness and columnar size distribution of the El Chichón stratospheric aerosol layer, *J. Geophys. Res.*, *90*, 10,607–10,619.
- Stevenson, D. S., C. E. Johnson, W. J. Collins, R. G. Derwent (2003), The tropospheric sulphur cycle and the role of volcanic SO₂, in *Volcanic Degassing*, edited by C. Oppenheimer, D. M. Pyle, and J. Barclay, *Geol. Soc. Spec. Publ.*, *213*, 295–305.
- Stüth, J. L., P. V. Hobbs, and L. F. Radke (1978), Airborne particle and gas measurements in the emissions from six volcanoes, *J. Geophys. Res.*, *83*, 4009–4017.
- Symonds, R. B., W. I. Rose, and M. H. Reed (1988), Contribution of Cl⁻ and F⁻ bearing gases to the atmosphere by volcanoes, *Nature*, *334*, 415–418.
- Tang, I. N., and H. R. Munkelwitz (1994), Water activities, densities, and refractive indices of aqueous sulfates and sodium nitrate droplets of atmospheric importance, *J. Geophys. Res.*, *99*, 18,801–18,808.
- Tomasi, C., V. Vitale, and L. Tarozzi (1997), Sun-photometric measurements of atmospheric turbidity variations caused by the Pinatubo aerosol cloud in the Himalayan region during the summer periods of 1991 and 1992, *Nuovo Cimento Soc. Ital. Fis. C*, *20*, 61–88.
- Twomey, S. (1963), On the numerical solution of Fredholm integral equations of the first kind by the inversion of the linear system produced by quadrature, *J. Assoc. Comput. Mach.*, *10*, 97–101.
- van de Hulst, H. C. (1957), *Light Scattering by Small Particles*, John Wiley, Hoboken, J. J.
- Watson, I. M., and C. Oppenheimer (2000), Particle size distributions of Mount Etna's aerosol plume constrained by Sun photometry, *J. Geophys. Res.*, *105*, 9823–9829.
- Watson, I. M., and C. Oppenheimer (2001), Photometric observations of Mt. Etna's different aerosol plumes, *Atmos. Environ.*, *35*, 3561–3572.
- Witter, J. B., and E. S. Calder (2004), Magma degassing at Villarrica Volcano, in *Villarrica Volcano, SERNAGEOMIN Special Bulletin*, edited by J. Clavero and L. Lara, Serv. Nac. de Geol. y Miner., Santiago, Chile, in press.
- Witter, J. B., V. C. Kress, P. Delmelle, and J. Stix (2004), Volatile degassing, petrology, and magma dynamics of the Villarrica lava lake, southern Chile, *J. Volcanol. Geotherm. Res.*, *134*, 303–337.
- Wooster, M. J. (2001), Long-term infrared surveillance of Lascar Volcano: Contrasting activity cycles and cooling pyroclastics, *Geophys. Res. Lett.*, *28*, 847–850.
- Wooster, M. J., and D. A. Rothery (1997), Thermal monitoring of Lascar Volcano, Chile using infrared data from the along-track scanning radiometer: A 1992–1995 time-series, *Bull. Volcanol.*, *58*, 566–579.
- Yamamoto, G., and M. Tanaka (1969), Determination of aerosol size distributions from spectral attenuation measurements, *Appl. Opt.*, *8*, 447–453.
- Yang, P., M. G. Mlynczak, H. Wei, D. P. Kratz, B. A. Baum, Y. X. Hu, W. J. Wiscombe, A. Heidinger, and M. I. Mishchenko (2003), Spectral signature of ice clouds in the far-infrared region: Single-scattering calculations and radiative sensitivity study, *J. Geophys. Res.*, *108*(D18), 4569, doi:10.1029/2002JD003291.

A. G. Allen, School of Geography, Earth and Environmental Sciences, University of Birmingham, Edgbaston, Birmingham B15 2TT, UK.

T. A. Mather and D. M. Pyle, Department of Earth Sciences, University of Cambridge, Downing Street, Cambridge CB2 3EQ, UK. (tam21@cam.ac.uk)

A. J. S. McGonigle, C. Oppenheimer, and V. I. Tsanev, Department of Geography, University of Cambridge, Downing Place, Cambridge CB2 3EN, UK.